Molecular Therapy
Oncolytics
Original Article

Humanized Mice with Subcutaneous Human Solid Tumors for Immune Response Analysis of Vaccinia Virus-Mediated Oncolysis

Desislava Tsoneva,[1] Boris Minev,[2,3] Alexa Frentzen,[3] Qian Zhang,[3] Anja K. Wege,[4] and Aladar A. Szalay[1,2,3,5]

[1]Department of Biochemistry, Biocenter, University of Wuerzburg, 97074 Wuerzburg, Germany; [2]Department of Radiation Medicine and Applied Sciences, Rebecca & John Moores Comprehensive Cancer Center, University of California, San Diego, CA 92093, USA; [3]Genelux Corporation, San Diego Science Center, San Diego, CA 92109, USA; [4]Department of Gynecology and Obstetrics, University Medical Center Regensburg, 93053 Regensburg, Germany; [5]Rudolph Virchow Center for Experimental Biomedicine, University of Wuerzburg, 97080 Wuerzburg, Germany

Oncolytic vaccinia virus (VACV) therapy is an alternative cancer treatment modality that mediates targeted tumor destruction through a tumor-selective replication and an induction of anti-tumor immunity. We developed a humanized tumor mouse model with subcutaneous human tumors to analyze the interactions of VACV with the developing tumors and human immune system. A successful systemic reconstitution with human immune cells including functional T cells as well as development of tumors infiltrated with human T and natural killer (NK) cells was observed. We also demonstrated successful in vivo colonization of such tumors with systemically administered VACVs. Further, a new recombinant GLV-1h376 VACV encoding for a secreted human CTLA4-blocking single-chain antibody (CTLA4 scAb) was tested. Surprisingly, although proving CTLA4 scAb's in vitro binding ability and functionality in cell culture, beside the significant increase of CD56^{bright} NK cell subset, GLV-1h376 was not able to increase cytotoxic T or overall NK cell levels at the tumor site. Importantly, the virus-encoded β-glucuronidase as a measure of viral titer and CTLA4 scAb amount was demonstrated. Therefore, studies in our "patient-like" humanized tumor mouse model allow the exploration of newly designed therapy strategies considering the complex relationships between the developing tumor, the oncolytic virus, and the human immune system.

INTRODUCTION

According to the World Health Organization, cancer is responsible for estimated 8 million of deaths worldwide with the number of new cancer cases expected to rise from approximately 14 million to over 20 million annually within the next two decades.[1] The inability of conventional cancer treatment modalities such as surgery, chemotherapy, and radiation therapy to cure or even to significantly extend the life of cancer patients requires development of new, less invasive, and more effective cancer treatment options, which can be used alone or in combination with the conventional therapies.

A promising new approach for the treatment of cancer is the use of oncolytic viruses, which exhibit a natural tumor tropism and oncolysis that could be further genetically enhanced.[2,3] One of the top candidates in this area are the oncolytic vaccinia viruses (VACVs), which selectively infect and destroy tumor cells as a result of viral replication and stimulation of the host immune response, while sparing surrounding healthy cells and tissues.[4–6] The use of VACV in the smallpox eradication campaign[7,8] provided important information on its behavior in humans, making it the virus with the longest and the most extensive use in our society. The injection of the virus into the bloodstream and its systemic delivery into solid tumors and their metastases in mouse models have already shown extremely promising results.[9–12] Recombinant vaccinia virus (rVACV) strains are also among the main contenders with oncolytic properties that are currently being evaluated in clinical trials.[4,13,14] However, due to differences in innate and adaptive immunity between mice and humans,[15] studying the interactions between VACV-colonized tumors and murine immune system is not directly representative for these interactions in human cancer patients. Further, ethical and legal concerns as well as risk of potential toxicity limit research involving human patients. Therefore, a suitable in vivo model for testing interactions between VACV-colonized human tumors and human immune cells, avoiding the numerous limitations and risks associated with cell culture, animal models, and human studies, is the humanized tumor mouse model.

The advances in murine genetics during the last 30 years led to the development of new immunodeficient mouse models that allowed successful engraftment with human hematopoietic stem cells.[16–22] The highest levels of human immune system reconstitution after human CD34^{+} progenitor cell transplantation in newborn mice[23,24] were observed in the highly immunodeficient NOD/SCID/IL2rγ^{null} (NSG) mouse strain.[25] In 2011, Wege et al. reported the first humanized tumor mouse model,[26] which involves a co-transplantation of

Received 1 September 2016; accepted 2 March 2017;
http://dx.doi.org/10.1016/j.omto.2017.03.001.

Correspondence: Aladar A. Szalay, University of Wuerzburg, Biochemistry Am Hubland, Wuerzburg 97074, Germany.
E-mail: szalay@biozentrum.uni-wuerzburg.de

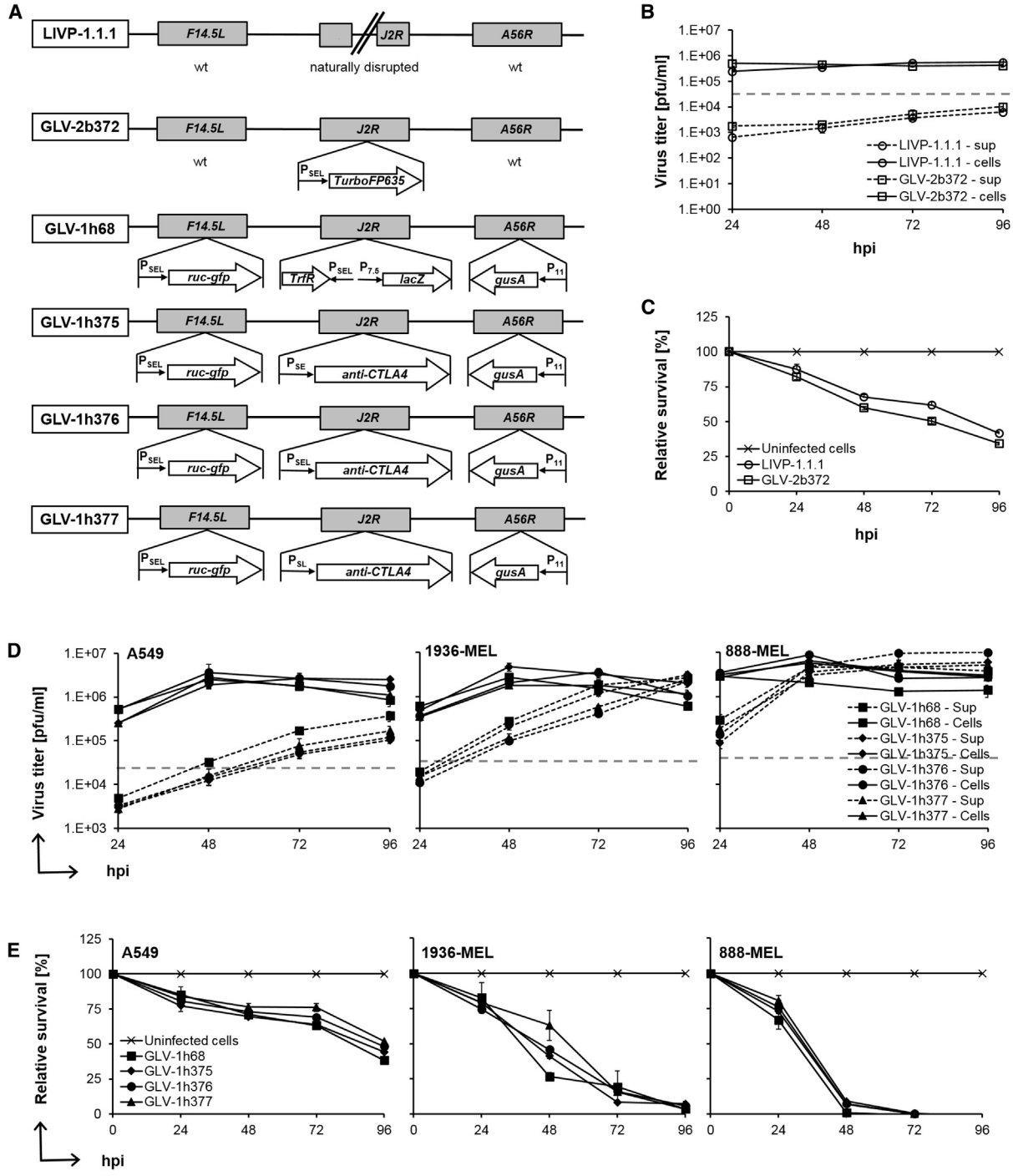

Figure 1. VACV Constructs, Replication, and Cytotoxicity Assays

(A) Schematic representation of VACV constructs and marker genes. LIVP-1.1.1 is an isolate from the WT LIVP with naturally disrupted *J2R* locus. GLV-2b372 was delivered from LIVP-1.1.1 by inserting the far-red fluorescent protein TurboFP635 (*TurboFP635*) expression cassette into the *J2R* locus under the control of the VACV synthetic early/late promoter (P_{SEL}). The recombinant VACV strain GLV-1h68 was constructed as specified by Zhang et al.[10] GLV-1h375, -1h376, and -1h377 were delivered from GLV-1h68 by replacing the *TrfR lacZ* expression cassette at the *J2R* locus with the anti-human CTLA4 FLAG-tagged single-chain antibody (*anti-CTLA4*) expression cassette under three different VACV synthetic early (P_{SE}), early/late (P_{SEL}), and late (P_{SL}) promoters, respectively. (B and D) Replication assay. Human A549 or A549, 1936-MEL, and 888-MEL cell cultures were infected with LIVP-1.1.1 (open circle) and GLV-2b372 (open squares) or GLV-1h68 (squares), -1h375 (diamonds), -1h376 (circles), and -1h377

(legend continued on next page)

human CD34$^+$ and cancer cells into the liver of newborn NSG mice resulting in a stable, long-term, multilineage reconstitution of a functional human immune system and at the same time development of solid tumors and tumor metastases without signs of rejection. However, a preliminary experiment with this model in our laboratory showed that injection of tumor cells into the liver of newborn NSG mice leads to the development of many large tumors in different mouse organs before multilineage human hematopoietic reconstitution with developed T cells could be detected in peripheral mouse blood. Further, the development of the tumors in the abdominal cavity did not allow precise caliper measurements or imaging of their size needed to assess the efficacy of the oncolytic treatment with VACV.

Therefore, a specific aim of this study was to establish a humanized tumor mouse model with subcutaneous human tumors. Such a small animal model may allow the evaluation of the oncolytic properties of VACV by direct monitoring of the size and colonization of the subcutaneous tumors after virus administration and at the same time the interactions of VACV with the host immune cells in the context of the human immune system in live mice. To develop such a model, we intrahepatically transplanted newborn NSG mice with human-cord-blood-derived CD34$^+$ hematopoietic stem cells, as previously described.[26] Subsequently, we studied whether subcutaneous implantation of human A549 lung cancer cells at 9–13 weeks post-humanization would result in a progressive tumor growth. We also examined whether treatment of these tumor-bearing humanized mice with different oncolytic VACV strains will in fact result in a successful selective colonization of the human tumors. We further applied this mouse model to characterize the human immune cells present in tumors and organs of virus-treated or control mice, as well as to analyze the effect of a rVACV-encoded human CTLA4-blocking single-chain antibody (CTLA4 scAb) on the activation status of the human T cells. Further, we studied the potential of β-glucoronidase assay, well-established in our laboratory,[27–29] to be used as a less time- and labor-consuming alternative for determination of viral titer and CTLA4 scAb concentration in humanized-mouse-derived samples instead of replication assay and ELISA.

RESULTS

VACV Strains Replicated Efficiently in All Tested Tumor Cell Lines

Schematic diagrams of the VACV strains used in this study are shown in Figure 1A. The wild-type (WT) LIVP-1.1.1 virus was used to study the effect of the VACV on the reconstituted human immune system in the humanized mouse model in the absence of any potentially immunogenic inserted genes. The insertion of the far-red fluorescent protein TurboFP635 (*TurboFP635*) expression cassette into the naturally disrupted *J2R* locus of the LIVP-1.1.1 virus led to the generation of the GLV-2b372 strain, which allowed monitoring of the virus distribution after systemic administration in mice. As a next step, one of the three newly engineered anti-human CTLA4 scAb-encoding VACVs, GLV-1h375, -1h376, or -1h377, was tested to evaluate the effect of the immune checkpoint blocker in the humanized mouse model. Their parental strain GLV-1h68 was utilized as a CTLA4 scAb^{negative} control. Before the application of these VACV strains in mice, they were evaluated in cell culture.

To determine the ability of those viruses to infect and replicate in cancer cell lines, cells were infected at an MOI of 0.1, and supernatants and cell lysates of infected cultures were collected separately and in triplicates at 24, 48, 72, and 96 hr post-infection (hpi), followed by standard plaque assay in CV-1 cell monolayers. Replication efficiency of LIVP-1.1.1 was tested in numerous tumor cell lines in cell culture and in mouse models[30–33] and was therefore here evaluated only in the susceptible-to-VACV human lung cancer cell line A549 (Figure 1B), used in the current study to generate the humanized subcutaneous tumor-bearing NSG mice. To examine whether insertion of the *TurboFP635* expression cassette into the *J2R* locus affects the replication of the GLV-2b372 virus compared to the parental LIVP-1.1.1 strain, additional infection studies were carried out. We found that both strains replicated efficiently and showed comparable titers over the time. Already, at 24 hpi viral titers of $2.53 \times 10^5 \pm 5.41 \times 10^{\circ}$ (LIVP-1.1.1) and $5.08 \times 10^5 \pm 2.35 \times 10^0$ (GLV-2b372) PFUs per milliliter (PFUs/mL) in cell lysates alone were higher than the infection medium. Viral titers in the supernatants of infected cultures steadily increased over time, reaching maximum values of $6.50 \times 10^3 \pm 7.07 \times 10^{-1}$ and $1.05 \times 10^4 \pm 6.48 \times 10^0$ PFUs/mL for LIVP-1.1.1 and GLV-2b372, respectively, at 96 hpi.

To examine whether the insertion of the expression cassette for the CTLA4 scAb in the *J2R* locus affects the infectivity and the replication efficiency of GLV-1h375, -1h376, and -1h377 VACV strains compared to the parental GLV-1h68 virus, infection studies were carried out in human A549, 1936-MEL, and 888-MEL cancer cell lines (Figure 1D). The pair of melanoma cell lines is an excellent model system as both lines were derived from the same patient with melanoma over a decade of observation,[34,35] which allows unique comparison of VACV effectiveness in targeting cancer cell lines with different tumor antigen expression levels and different chromosomal instability and responsiveness to immunotherapy. GLV-1h68 and its derivatives showed comparable replication; however, replication efficiency among cell lines slightly varied. Most susceptible to VACV replication were the 888-MEL cells, followed by 1936-MEL and A549 cells with mean total (sum of supernatant and cell lysate values) viral titers from all four virus strains tested of $8.72 \times 10^6 \pm 1.8 \times 10^6$, $3.80 \times 10^6 \pm 5.11 \times 10^5$, and $1.75 \times 10^6 \pm 3.78 \times 10^5$ PFUs/mL, respectively, reached at 96 hpi. Already, at 24 hpi PFUs in wells of the infected cell lines were 13- to 83-fold higher than those in the infection medium.

(triangles), respectively, at an MOI of 0.1. To determine replication efficiency, supernatants and cell lysates of infected cells were collected separately and in triplicates at 24, 48, 72, and 96 hpi. Viral titers were determined as PFUs per milliliter (PFUs/mL) of medium by standard plaque assay in CV-1 cell monolayers and plotted against the course of time. Mean values (n = 3) and SEM are plotted. (C and E) Viability of infected cells was monitored in triplicates over 96 hr using an MTT assay. Viable cells were calculated as percentage from the mock-infected control cells for each time point, which were considered to be 100% viable. Mean values (n = 3) and SEM are plotted.

Viral loads in most cell lysates peaked at 48 hpi, with the highest value of $8.83 \times 10^6 \pm 3.56 \times 10^0$ PFUs/mL observed in GLV-1h376-infected 888-MEL cells, followed by a slow decrease. Viral loads in the supernatants steadily increased over time, reaching maximum values at 96 hpi, with highest titer of $1.00 \times 10^7 \pm 7.35 \times 10^0$ PFUs/mL measured in the supernatants of GLV-1h376-infected 888-MEL cells.

These data confirmed that GLV-2b372 and GLV-1h375, -1h376, and -1h377 viruses were able to infect and to efficiently replicate in all tested cancer cell lines in a time-dependent fashion and in a similar manner to the parental strains LIVP-1.1.1 and GLV-1h68, respectively.

VACV Strains Efficiently Lysed Human Cancer Cell Lines

To assess whether TurboFP635 and CTLA4 scAb expression affects the oncolytic efficacy of GLV-2b372 and GLV-1h375, -1h376, and -1h377, respectively, compared to their parental viruses, A549, 1936-MEL, or 888-MEL human cancer cell lines were infected at an MOI of 0.1, and cytotoxicity was analyzed over 96 hr after infection by (3-(4,5-Dimethyl-2-thiazolyl)-2,5-diphenyl-2H-tetrazolium bromide (MTT) assays. GLV-2b372 virus killed the A549 cancer cells in a time-dependent fashion and in a similar manner to the parental LIVP-1.1.1 virus (Figure 1C). At 96 hpi, only 34.31% ± 0.05% and 41.53% ± 0.08% of the cancer cells survived after treatment with GLV-2b372 or LIVP-1.1.1, respectively. GLV-1h375, -1h376, and -1h377 viruses also showed considerable cytotoxic effect on the tested cancer cell lines, which increased over time and followed similar path as that of the parental GLV-1h68 strain (Figure 1E). The greatest cytotoxicity was observed in the 888-MEL cell line, where only 5.95% ± 2.07% of the cells were still viable after just 48 hr of infection. In contrast to the 1936-MEL cell line, where only 4.88% ± 1.10% of the cells survived at 96 hpi, in the most resistant to VACV replication A549 cell line 45.61% ± 3.36% of cells remained viable. These results confirmed the oncolytic efficacy of the recombinant VACV strains and correlated well with the replication efficiency data.

CTLA4 scAb Was Expressed in GLV-1h376-Infected A549 Cells and Secreted into the Culture Supernatant

In the newly constructed GLV-1h375, -1h376, and -1h377 rVACV strains, expression cassette for CTLA4 scAb was inserted in the *J2R* locus downstream of the VACV synthetic early (P_{SE}), early/late (P_{SEL}), and late (P_{SL}) promoters, respectively. In order to verify CTLA4 scAb expression and its secretion into the culture supernatants, A549 cells were infected at an MOI of 1 with either one of the rVACV strains, the parental GLV-1h68 (CTLA4 $scAb^{negative}$) or mock-infected, and cell lysates and supernatants were tested for presence of CTLA4 scAb by western blot analysis (Figure 2A). Cells infected with the CTLA4 scAb-encoding viruses showed a specific protein of the expected size of 29.81 or 27.46 kDa in cell lysates or supernatants, respectively. Immunoglobulin (Ig) kappa-chain leader sequence is available only in the intracellular protein and is removed upon secretion, responsible for the slightly smaller size of the secreted single-chain antibody. Highest expression and secretion levels of CTLA4 scAb were observed in cell lysates and supernatants of cultures infected with GLV-1h376 with the strongest P_{SEL} promoter, followed by -1h377 and -1h375 with the P_{SL} and P_{SE} promoters, respectively. No protein of this size was detected in GLV-1h68- or mock-infected control cells. These results confirmed that the CTLA4 scAb protein was successfully expressed in and secreted from infected human lung carcinoma A549 cells in cell culture. Because highest expression levels of CTLA4 scAb were detected in GLV-1h376-infected cells, GLV-1h376 was the virus of choice used in all subsequent experiments.

Affinity of Purified CTLA4 scAb to Human CTLA4 and Lack of Cross-Reactivity to Mouse CTLA4 In Vitro

The VACV-encoded CTLA4 scAb was constructed to be human specific with no cross-reactivity to mouse CTLA4. Since the affinity of CTLA4 scAb to human CTLA4 has not been characterized yet, we successfully purified the single-chain antibody from the supernatants of GLV-1h376-infected CV-1 cells (Figure 2B) and tested its binding to recombinant human CTLA4 (rh CTLA4) Fc chimera by ELISA (Figure 2C). A recombinant mouse CTLA4 (rm CTLA4) Fc chimera was used as a negative control. As expected, the CTLA4 scAb successfully recognized and was able to bind to rh CTLA4 Fc chimera. Lack of cross-reactivity between the antibody and the recombinant mouse peptide was confirmed.

The Purified CTLA4 scAb Is Functional in Cell Culture

Next, the functionality of the purified CTLA4 scAb was tested in cell culture. Jurkat cells were activated with a mix of phorbol 12-myristate 13-acetate (PMA), Ionomycin, and B7-1 and B7-2 proteins or with human T cell activation beads, and the ability of CTLA4 scAb to further increase the expression of early CD69 and late CD25 activation markers on activated cells was examined by flow cytometry. Images of representative dot plots from the analysis are shown in Figure 2D. Because Jurkat cells are an immortalized line of human T lymphocytes, which continuously proliferate, a relatively strong early CD69 (60%) and to a lesser extent late CD25 (4%) activation marker expression was observed even in the non-activated control cells (Figure 2E). Stronger expression of CD69 or CD25, approximately 89% and 23%, respectively, was detected in both mix- and bead-activated groups. As expected, the substitution of the activation reagents with purified CTLA4 scAb resulted in an increased T cell activation in both groups, with almost 100% of the cells expressing CD69 and approximately 70% of them expressing CD25.

Taken together, our data indicated that purified GLV-1h376-encoded CTLA4-blocking single-chain antibody was human CTLA4 specific and successfully enhanced Jurkat cell activation in cell culture. Such increased activation would be a result of the ability of CTLA4 scAb to bind to the cell-surface CTLA4 and therefore to block the inhibitory signaling through it.

Analysis of Virus-Mediated TurboFP635 and GFP Expression in Cell Culture and in Human Tumors from Humanized Mice

To evaluate the expression of the reporter proteins TurboFP635 and GFP in cell culture, human lung carcinoma A549 cells were infected

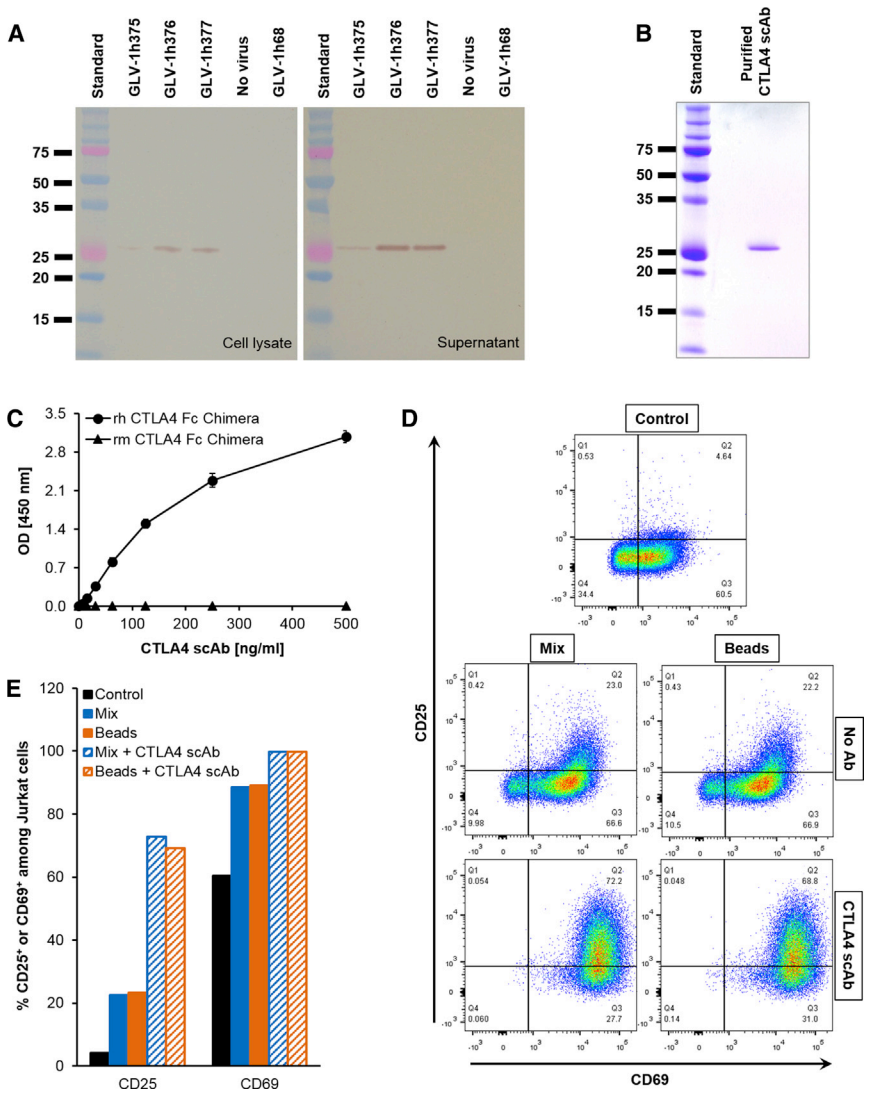

Figure 2. Overexpression, Purification, Affinity, and Functionality of Virus-Mediated CTLA4 scAb

(A) A549 cells were infected with rVACV strains at an MOI of 1. Cell lysates and supernatants of infected cultures were collected 24 hr later, and 4 and 10 μg of protein, respectively, were separated by SDS-PAGE. Intracellular and secreted FLAG-tagged CTLA4 scAb with the expected size of 29.81 and 27.46 kDa, respectively, was detected in the western blots using an anti-DDDDK antibody. Lines show standard band in kilodaltons. (B) CV-1 cell cultures were infected with GLV-1h376 at an MOI of 2. Supernatant was harvested 24 hr later and concentrated. CTLA4 scAb was purified using affinity gel. To verify its purity, a sample of the eluted scAb was separated by SDS-PAGE and stained with Coomassie brilliant blue. A Coomassie-stained gel shows the purified CTLA4 scAb. (C) Affinity of VACV-encoded and purified CTLA4 scAb and its lack of cross-reactivity were demonstrated by ELISA. 96-well plates were coated with recombinant human CTLA4 (rh CTLA4) Fc chimera (circles) or recombinant mouse CTLA4 (rm CTLA4) Fc chimera (triangles). Absorbance (OD) obtained for various CTLA4 scAb concentrations against both human and mouse Fc chimeras is plotted. Mean values (n = 3) and SEM are shown. (D and E) Jurkat cells were activated with a mix of PMA, Ionomycin, B7-1, and B7-2 or with commercially available T cell activation beads, alone, or additionally supplemented with purified CTLA4 scAb. Untreated samples of Jurkat cells were left as a control. Forty-eight hours later, all samples were analyzed in duplicates for early CD69 and late CD25 activation marker expression by flow cytometry. Images of representative dot plots (D) and corresponding bar graphs (E) are shown.

with the rVACV strains GLV-2b372 or GLV-1h68 and -1h376, respectively, at an MOI of 0.1 (Figure 3A). Fluorescent protein expression as a marker for viral infection and replication was assessed daily at 24, 48, 72, and 96 hpi by fluorescence microscopy. Cells infected with all three viruses were found to express the marker proteins by 24 hpi; however, expression increased in a time-dependent manner over the first 72 hr after the infection followed by a decline due to the oncolytic effect of the virus. GFP expression levels in GLV-1h376-infected cells changed in a similar manner to those in cells infected with the parental GLV-1h68 virus. The results from the fluorescent microscopy correlate well with the virus replication and cytotoxicity data and demonstrate that the fluorescent marker protein expression in rVACV-infected tumor cells could be used to monitor the virus replication in cell culture.

The successful colonization of subcutaneous A549 human tumors in humanized NSG mice with recombinant TurboFP635-encoding GLV-2b372 VACV strain after systemic administration of 6×10^6 PFUs was visualized at 3, 8, and 15 days post infection (dpi) by fluorescent imaging of live animals (Figure 3B). Tumors in all virus-treated mice were positive for TurboFP635. We observed an initial 22-fold increase of fluorescent signal during the first 8 days of the infection and consequent decrease in TurboFP635 expression by day 15 (Figure 3B, right panel). Obtained data demonstrated that the rVACV strain GLV-2b372 was able to specifically infect and efficiently replicate in A549 tumors after systemic administration, as well as that rVACV-encoded fluorescent marker proteins could successfully be used for real-time, non-invasive monitoring of virus replication in live-tumor-bearing humanized NSG mice.

Furthermore, we also evaluated GFP as a marker for successful tumor colonization in excised A549 tumors from humanized NSG mice 10 days after systemic administration of 6×10^6 PFUs of GLV-1h376 or its parental strain GLV-1h68 (Figure 3C). Expression of GFP in tumors was visualized by direct fluorescent microscopy ex vivo. In fact, tumors from all rVACV-treated mice were found positive for GFP.

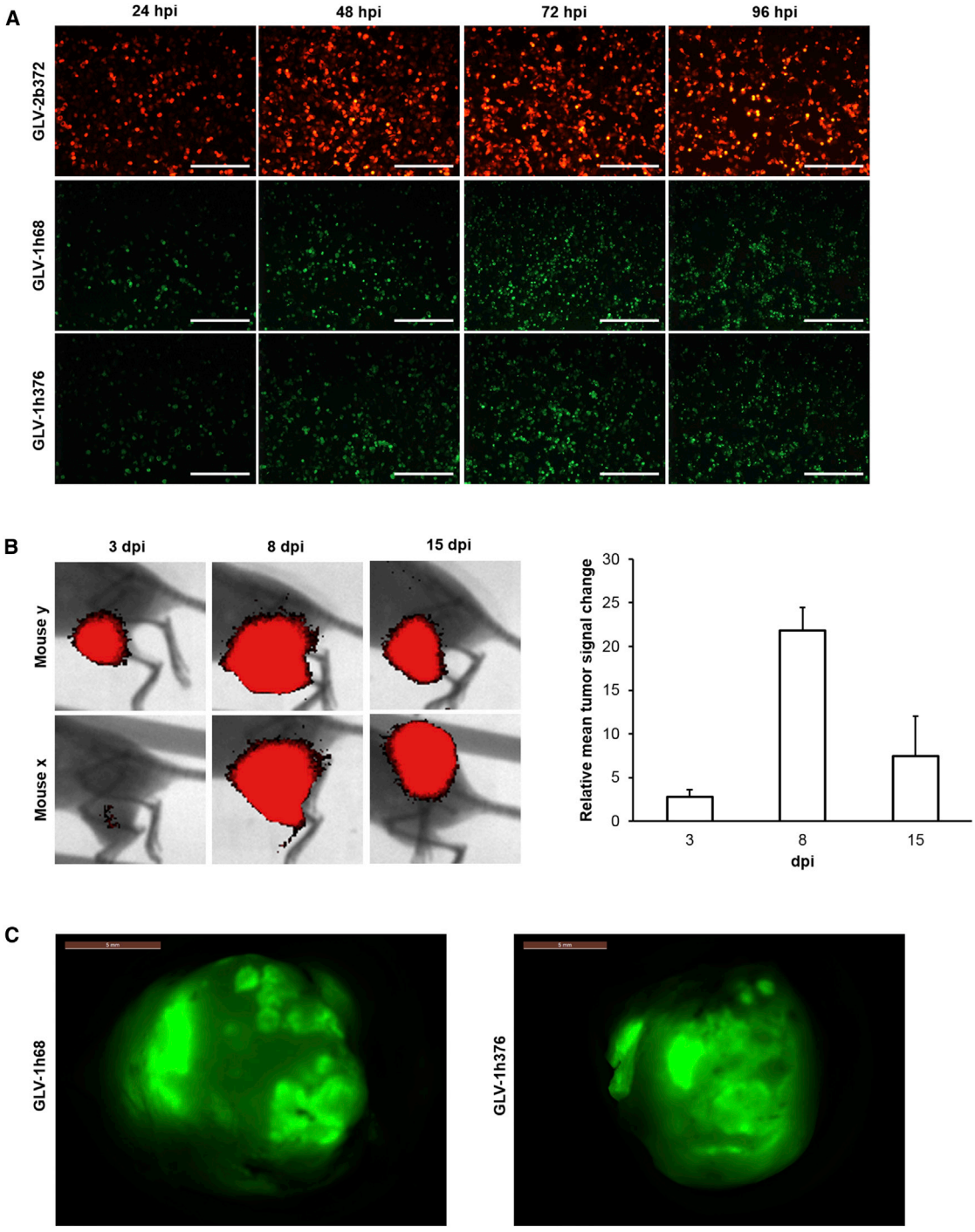

Figure 3. VACV-Mediated Fluorescent Protein Expression in Tumor Cell Culture and in Tumors

(A) A549 cell cultures were infected with GLV-2b372, GLV-1h68, or -1h376 at an MOI of 0.1 and monitored over 96 hr. TurboFP635 and GFP expression in infected cell cultures was visualized by direct fluorescent microscopy and increased in a time-dependent fashion. Scale bar, 500 μm. (B) A549-tumor-bearing humanized NSG mice were injected retro-orbitally (r.o.) with 6×10^6 viral particles of GLV-2b372. Animals were imaged for TurboFP635 expression at 3 (n = 4), 8 (n = 3), and 15 (n = 3) dpi. The images show the tumor area of two representative mice. The TurboFP635 signal from the GLV-2b372 colonized A549 tumors was measured in relative fluorescence units. Relative tumor signal change was monitored over 15 dpi. Mean values and SEM are plotted. (C) A549-tumor-bearing humanized NSG mice were injected r.o. with 6×10^6 viral particles of GLV-1h68 or -1h376. Ten-dpi tumors were excised and examined for GFP expression by direct fluorescent microscopy. Representative pictures from both virus groups are shown. Scale bar, 5 mm.

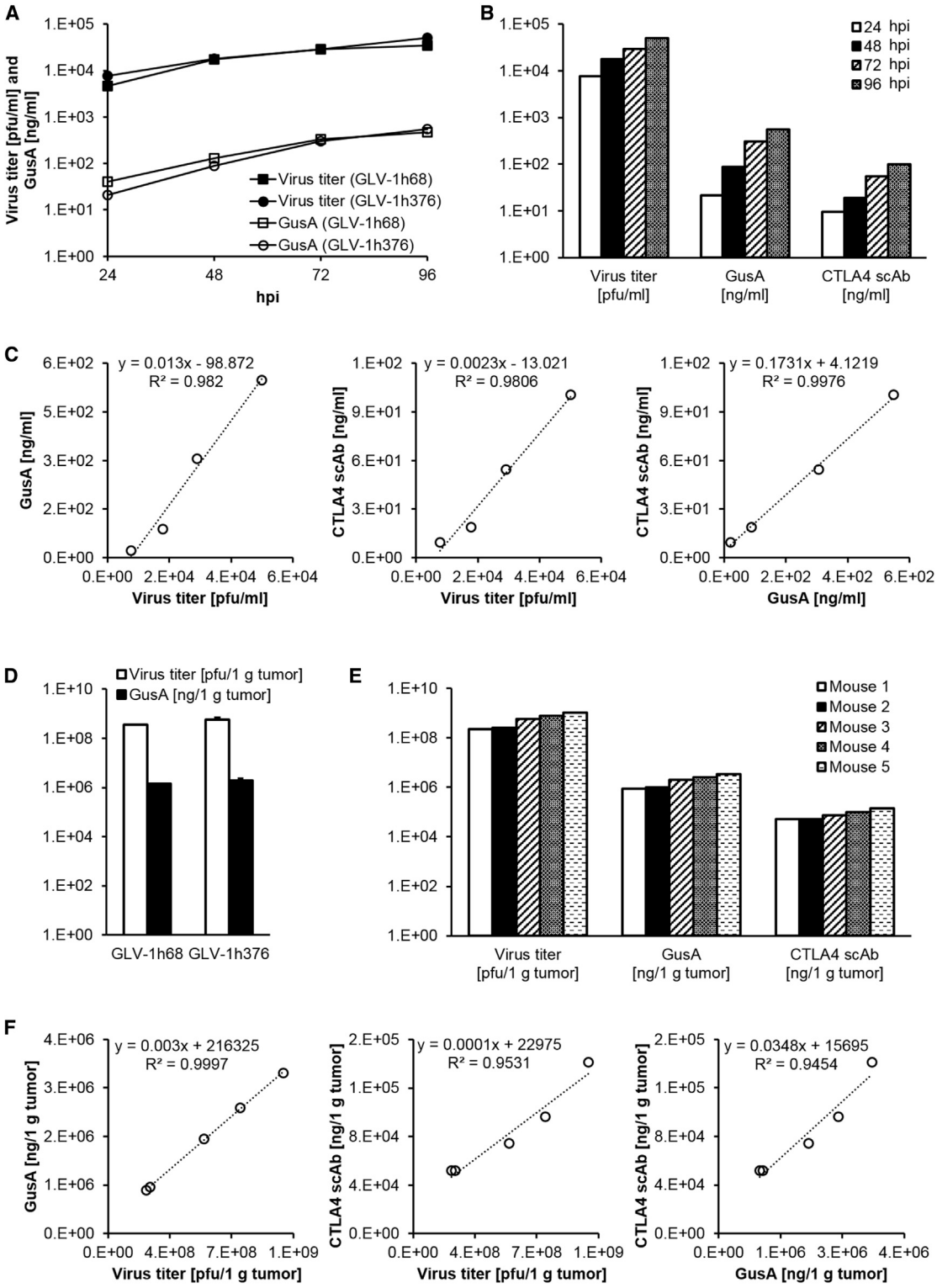

Figure 4. CTLA4 scAb and β-Glucuronidase Expression in GLV-1h376-Infected A549 Cell Cultures or Subcutaneous Tumors

(A–C) A549 cell cultures were infected with GLV-1h376 or the control GLV-1h68 (CTLA4 scAb^{negative}) strain at an MOI of 0.005. Supernatants and cell lysates of infected cells were harvested separately and in triplicates at 24, 48, 72, and 96 hpi. After collecting all time points, samples were assayed for PFUs, β-glucuronidase (GusA), and CTLA4

(legend continued on next page)

GLV-1h376-Virus-Mediated β-Glucuronidase and CTLA4 scAb Expression Levels Correlate with Viral Titers in Cell Culture and Humanized-Mouse-Derived Human Tumor Samples

The GLV-1h376 strain was used to compare the amounts of the rVACV-encoded CTLA4 scAb and β-glucuronidase (GusA) and to study their correlation with the plaque-forming units in A549 cells infected at an MOI of 0.005 for up to 96 hr. Collected supernatants and cell lysates from each time point were assayed separately for PFUs, GusA, and CTLA4 scAb by standard plaque assay, β-glucuronidase assay, and ELISA, respectively, and the sum values were presented per milliliter.

First, to evaluate whether the CTLA4 scAb expression affects the expression of the reporter protein GusA, GusA levels and viral titers in A549 cells infected with GLV-1h376 or the parental GLV-1h68 virus were compared (Figure 4A). Both VACV strains were found to efficiently replicate in A549 cells in culture. Viral titers showed a slight but constant increase during the course of the replication assays with comparable values reached at each time point. Although GLV-1h68 titer (4.62×10^3 PFUs/mL) at 24 hpi was slightly lower when compared to the GLV-1h376 titer (7.69×10^3 PFUs/mL), viral loads for both strains reached similar levels by 48 hpi. Increasing viral titers in the culture samples resulted also in increasing GusA protein levels throughout the whole assay. GusA concentration in GLV-1h68-infected cells (4.08×10^1 ng/mL) at 24 hpi was twice as high as in GLV-1h376-treated cells (2.12×10^1 ng/mL), but this difference faded with time, and they reached similar levels of 3.28×10^2 and 3.02×10^2 ng/mL, respectively, at 72 hpi. Taken together, difference in the expression of GLV-1h68- and -1h376-encoded GusA was observed only in the early stage of the virus infection and diminished as the infection progressed.

In GLV-1h376-infected cells, viral replication resulted in increasing virus-mediated GusA and CTLA4 scAb expression throughout the course of the assay (Figure 4B). An excellent correlation with correlation coefficient $R^2 = 0.9820$ or $R^2 = 0.9806$ was observed between GusA or CTLA4 scAb concentration, respectively, and the corresponding PFUs (Figure 4C). Because the concentrations of both virus-encoded proteins each correlated with viral replication, a good correlation between them was expected too. Indeed, the correlation coefficient between GusA and CTLA4 scAb amounts was $R^2 = 0.9976$. The excellent correlations indicate that each of the three parameters could be used to estimate the amount of the other two when tested in cell-culture samples. This also means that β-glucuronidase assay as the least time consuming and labor intensive of the three assays is sufficient to perform to calculate all three parameters.

Expression of CTLA4 scAb and/or GusA and their correlation with the viral titers were also analyzed by ELISA, β-glucuronidase assay, and standard plaque assay, respectively, in single-cell suspension from excised A549 tumors infected with GLV-1h376 or the parental GLV-1h68 virus. First, we examined whether in vivo GLV-1h376 might be less effective in colonizing tumors than GLV-1h68 (Figure 4D). Consistent with the results from the infected cell cultures, both VACVs could efficiently replicate in the A549 tumors of live humanized NSG mice and reached comparable viral loads at day 10 after the infection. Viral titers of 3.56×10^8 and 5.74×10^8 PFUs/1 g tumor and corresponding GusA concentrations of 1.43×10^6 and 1.94×10^6 ng/1 g tumor were observed for GLV-1h68 and -1h376, respectively.

In GLV-1h376-infected A549 tumors, higher viral loads corresponded to higher virus-mediated GusA and CTLA4 scAb expression (Figure 4E). An excellent correlation with correlation coefficient $R^2 = 0.9997$ or $R^2 = 0.9531$ was observed between GusA or CTLA4 scAb concentration, respectively, and viral titer (Figure 4F). Because both proteins correlated with viral replication, a good correlation between them was expected too. Indeed, the correlation coefficient between GusA and CTLA4 scAb concentrations was $R^2 = 0.9454$. The excellent correlations indicate that each of the three parameters could be used to estimate the amount of the other two when tested in humanized-mouse-derived tumor samples.

Macroscopic Analysis of Excised Tumors and Spleens

Subcutaneous implantation of 5×10^6 human lung carcinoma A549 cells into the right hind leg of non-humanized or humanized NSG mice resulted in a successful tumor growth in all implanted animals. Tumors and spleens from such non-humanized, humanized, or LIVP-1.1.1 vaccinia-virus-treated humanized A549-tumor-bearing NSG mice were excised at 18 weeks post-humanization, 5 weeks after tumor implantation and 8 days after virus administration, and macroscopically examined (Figure S1). Majority of the tumors from non-humanized and humanized NSG mice that have not been treated with VACV showed large fluid-filled necrotic areas, many blood vessels, and large hemorrhagic regions. In contrast, VACV-colonized humanized-mouse-derived tumors showed more compact structure, with fewer blood vessels and virtually no hemorrhagic areas.

Another interesting observation was the spleen size dependence on humanization and virus administration. Generally, humanized NSG

scAb by standard plaque assay, β-glucuronidase assay, and ELISA, respectively. Shown values per milliliter are the sum of the supernatant and cell lysate values. (A) Virus replication efficiency (circles and squares) and GusA expression pattern (open circles and squares) in GLV-1h376- and -1h68-infected cells, respectively. (B) Viral titer and GusA and CTLA4 scAb levels in GLV-1h376-treated cells during the time of the infection. (C) Correlation with correlation coefficients $R^2 > 0.9806$ were observed between virus titer, GusA, and CTLA4 scAb in GLV-1h376-infected cells. (D–F) A549-tumor-bearing humanized NSG mice were injected with GLV-1h68 (n = 5) or -1h376 (n = 5). Tumors were excised at 15 weeks post-humanization and 10 days after virus administration. Prepared single-cell suspensions were assayed for PFUs, GusA, and CTLA4 scAb by standard plaque assay, β-glucuronidase assay, and ELISA, respectively. Values are shown per 1 g of tumor tissue. (D) Virus titers (no fill) and GusA concentrations (solid fill) in GLV-1h376- and -1h68-colonized tumors. Mean values and SEM are plotted. (E) Virus titer and GusA and CTLA4 scAb concentrations in tumors from five GLV-1h376-treated mice. (F) Correlation with correlation coefficients $R^2 > 0.9454$ were observed between virus titer, GusA, and CTLA4 scAb in GLV-1h376-colonized tumors.

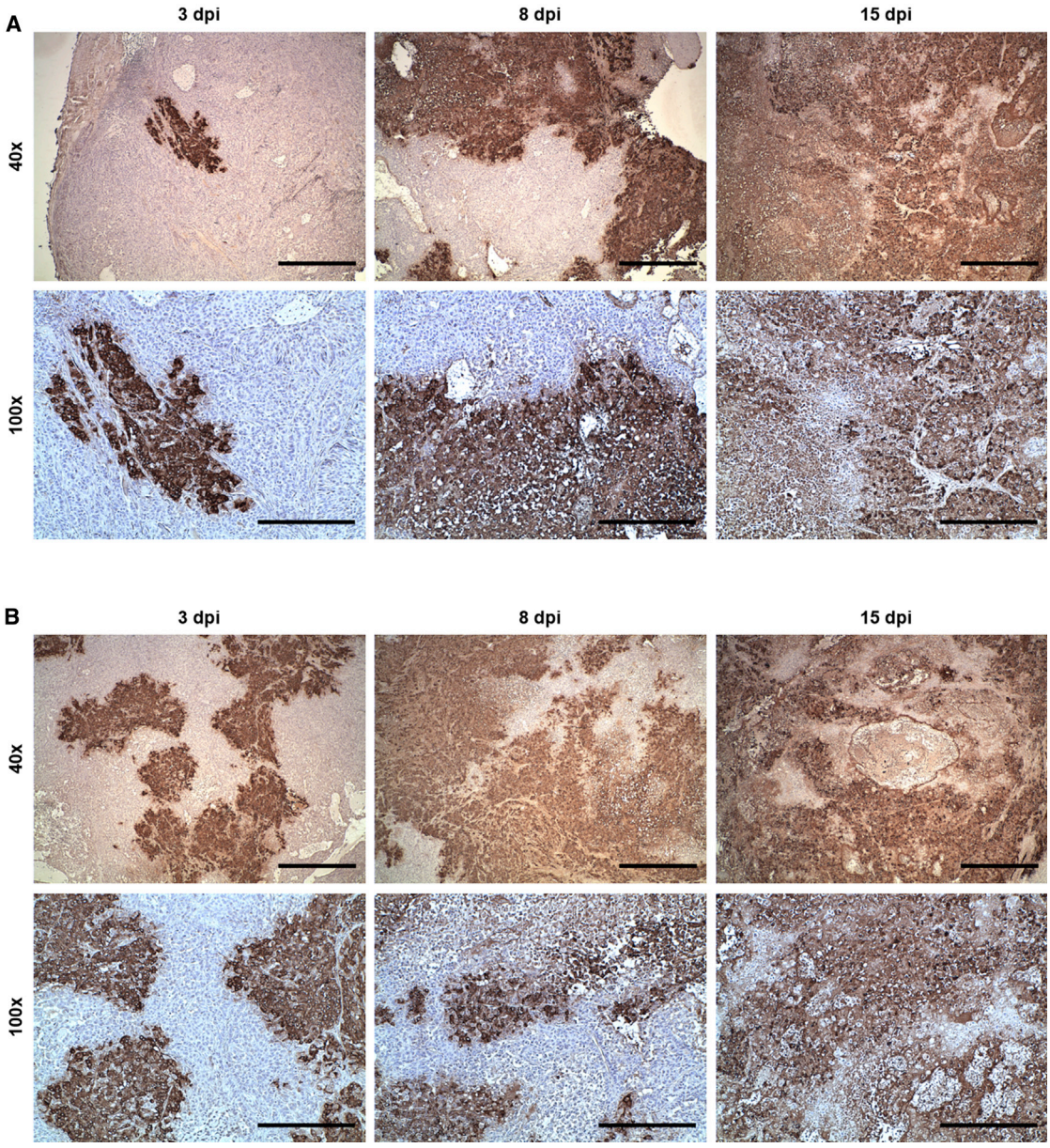

Figure 5. Immunohistochemical Analysis of Vaccinia-Virus-Colonized Tumors

A549-tumor-bearing humanized NSG mice were injected retro-orbitally with LIVP-1.1.1 or GLV-2b372 at 12 weeks post-humanization. At 3, 8, and 15 dpi, tumors from both mouse groups were excised for immunohistochemistry. Slides with tumor sections were stained for VACV and counterstained with hematoxylin. Tumor sections from representative LIVP-1.1.1- (A) or GLV-2b372- (B) injected mice obtained at 40× (scale bar, 1mm) and 100× (scale bar, 500 μm) magnification are shown.

mice had larger spleens compared to non-humanized NSG mice. Compared to humanized-mouse-derived spleens, enlarged spleens were observed in many of the VACV-treated humanized animals, suggesting a probable vaccinia-virus-induced splenomegaly.

Immunohistochemical Analysis of Vaccinia-Virus-Colonized Tumors

Immunohistochemical staining for the detection of VACV in tumor tissues from VACV-treated A549-tumor-bearing humanized NSG mice was performed to demonstrate the successful colonization of subcutaneous A549 tumors with LIVP-1.1.1 (Figure 5A) or GLV-2b372 (Figure 5B) after systemic virus administration and to investigate the progression of the infection and the corresponding histopathological changes in tumors. Time-dependent increase of VACV-infected tumor areas leading to tumor tissue destruction was observed for both virus strains. Small areas of virus infection were detected at 3dpi. These areas significantly increased in size by day 8 due to the fast virus spread. At the infection site, tumor cells rounded up and

detached, and tumor tissue had lost its integrity. At 15 dpi, virtually the whole sections were positive for VACV. Much more extensive necrotic regions and lesions were observed. Similar infection progression was observed for both viruses.

Both Human Natural Killer and T Cell Populations Are Present in Untreated or LIVP-1.1.1 VACV-Treated Non-tumorous Humanized NSG Mice

Blood and splenocytes collected from untreated and LIVP-1.1.1-treated non-tumorous humanized NSG mice 8 weeks post-humanization and 7 days after virus administration were analyzed for the presence of human natural killer (NK) and T cells by flow cytometry. We first investigated the NKp46 expression, which is exclusively expressed on resting and activated NK cells.[36–38] Human NK cell reconstitution was very low in blood and spleens of our model with an average of 2.21% ± 0.59% and 1.50% ± 0.31%, respectively (Figure S2A). LIVP-1.1.1 treatment non-significantly lowered the average percentage to 1.55% ± 0.25% in blood and 1.33% ± 0.29% in spleens. Consistent with previous reports,[26,39] further subset analysis of $NKp46^+$ NK cells revealed that both $CD56^-$ as well as $CD56^+$ cells were present in the organs from both groups. $NKp46^+CD56^+$ double-positive (DP) NK cells represented 51.70% ± 2.37% of the NK cells in the spleens but only 1.25% ± 0.34% in the blood, and LIVP-1.1.1 treatment did not significantly change the average percentage (Figure S2B). Two $NKp46^+CD56^+$ subpopulations were defined on the basis of the relative expression of the CD56 marker (bright versus dim expression). $CD56^{dim}$ cells were found to constitute the majority among DP cells in the peripheral blood (90.58% ± 1.24%) as well as in the spleens (92.19% ± 0.76%), and the virus treatment did not affect the overall percentage (88.11% ± 2.07% and 89.03% ± 1.46%, respectively) (Figure S2C). Further, both $CD4^+$ and $CD8^+$ T cells developed in this mouse model (Figure S2D). In order to detect their frequency, peripheral blood mononuclear cells (PBMCs) and splenocytes were gated on human CD45 → CD3 and then the respective lineage-specific marker. Although $CD4^+$ and $CD8^+$ T cells were detected in close percentage in blood (42.19% ± 6.76% and 44.66% ± 3.85%) and spleens (33.10% ± 6.03% and 50.27% ± 4.25%) of humanized mice, respectively, they significantly differed in the expression of the CD25 activation marker (Figure S2E). The percentage of $CD4^+CD25^+$ T cells reached 29.17% ± 4.02% in the blood and 38.71% ± 2.61% in the spleens, whereas only 1.88% ± 0.51% of $CD8^+$ T cell in the blood and 2.79% ± 0.31% in the spleens expressed CD25. Virus treatment did not significantly change the CD25 expression for either one of the T cell subsets in the tested samples.

Detection of Systemic Reconstitution with Human B, T, and NK Cells in Untreated or LIVP-1.1.1-Virus-Treated A549-Tumor-Bearing Humanized NSG Mice

Human B, T, and NK cell reconstitution in blood, spleens, and/or tumors of untreated or LIVP-1.1.1-treated A549-tumor-bearing humanized NSG mice 18 weeks post-humanization and 8 days after virus administration was analyzed by flow cytometry. First, $CD19^+$ B and $CD3^+$ T cell percentages among human $CD45^+$ cells were evaluated in the mouse peripheral blood to analyze the dynamics of the evolving humanization process in this model (Figure 6A). A significant change in the $CD19^+/CD3^+$ ratio was reported from day 59 to day 119 after humanization with a B cell decrease (from 84.96% ± 4.76% to 63.90% ± 4.04%) and a T cell increase (from 6.17% ± 4.98% to 27.43% ± 4.72%).

Consistent with the data obtained from the non-tumorous humanized mice (Figure S2), we found very low percentages of $NKp46^+$ NK cells among the human $CD45^+$ cells in blood and spleens of both untreated and LIVP-1.1.1-treated tumor-bearing mouse groups (Figure 6B). In contrast, NK cells were a much more abundant human immune cell type in tumors and represented 41.14% ± 10.56% and 27.57% ± 6.72% of the tumor-infiltrating human $CD45^+$ cells in untreated and LIVP-1.1.1 mouse groups, respectively. Virus administration did not significantly affect the overall $NKp46^+$ NK cell percentages in those tumors. The percentages of $CD56^+$ NK cells among the human $NKp46^+$ cells in blood (2.40% ± 0.53% and 0.78% ± 0.21%) and spleens (63.58% ± 3.45% and 61.83% ± 3.27%) of untreated and virus-treated tumor-bearing mice, respectively (Figure 6C), were very close to those seen in the non-tumorous humanized mice as well. Interestingly, 96.42% ± 1.07% of the $NKp46^+$ cells in tumors were expressing CD56; however, LIVP-1.1.1 treatment did not significantly change the average percentage (94.63% ± 1.32%). Even more, 86.74% ± 2.19% of the $CD56^+$ NK cells in tumors but only 6.80% ± 1.56% and 12.69% ± 4.00% of these cells in blood and spleens, respectively, were $CD56^{bright}$, and the virus treatment did not significantly affect the overall percentage (Figure 6D).

Regarding the T cell population, $CD4^+$ and $CD8^+$ T cells were detected in close percentage in blood (54.45% ± 3.18% and 38.78% ± 2.32%), spleen (45.48% ± 2.60% and 43.11% ± 2.49%), and tumors (44.73% ± 13.88% and 39.12% ± 13.77%), respectively (Figure 6E). Virus treatment slightly but significantly ($p < 0.05$) lowered the percentage of $CD4^+$ T cells and increased the percentage of $CD8^+$ T cells among splenocyte-derived $CD3^+$ T cells to 33.86% ± 3.80% and 52.01% ± 3.55%, respectively, but did not significantly affect the overall percentages in blood and tumors. In contrast, both T cell subsets substantially differed in the CD25 expression in the tested tissues (Figure 6F). $CD4^+CD25^+$ T cells were detected in similar percentages in blood (41.56% ± 4.33%) and spleen (39.73% ± 2.06%) but reached a much higher percentage in tumors (69.25% ± 6.39%). Interestingly, $CD8^+CD25^+$ T cells reached 54.19% ± 7.69% in tumors, whereas only 2.58% ± 0.69% of the $CD8^+$ T cell in blood and 1.82% ± 0.45% of these in spleens expressed CD25. Virus treatment did not significantly change the percentage of CD25-expressing cells for both T cell subsets in the tested samples.

Effect of VACV-Encoded CTLA4 Immune Checkpoint Inhibitor on Human Immune Cell Subsets in Humanized A549-Tumor-Bearing NSG Mice

Blood, spleens, and tumors collected from untreated and CTLA4 scAb-encoding GLV-1h376-virus- or parental GLV-1h68-virus-treated humanized NSG mice at 15 weeks post-humanization and 10 days after

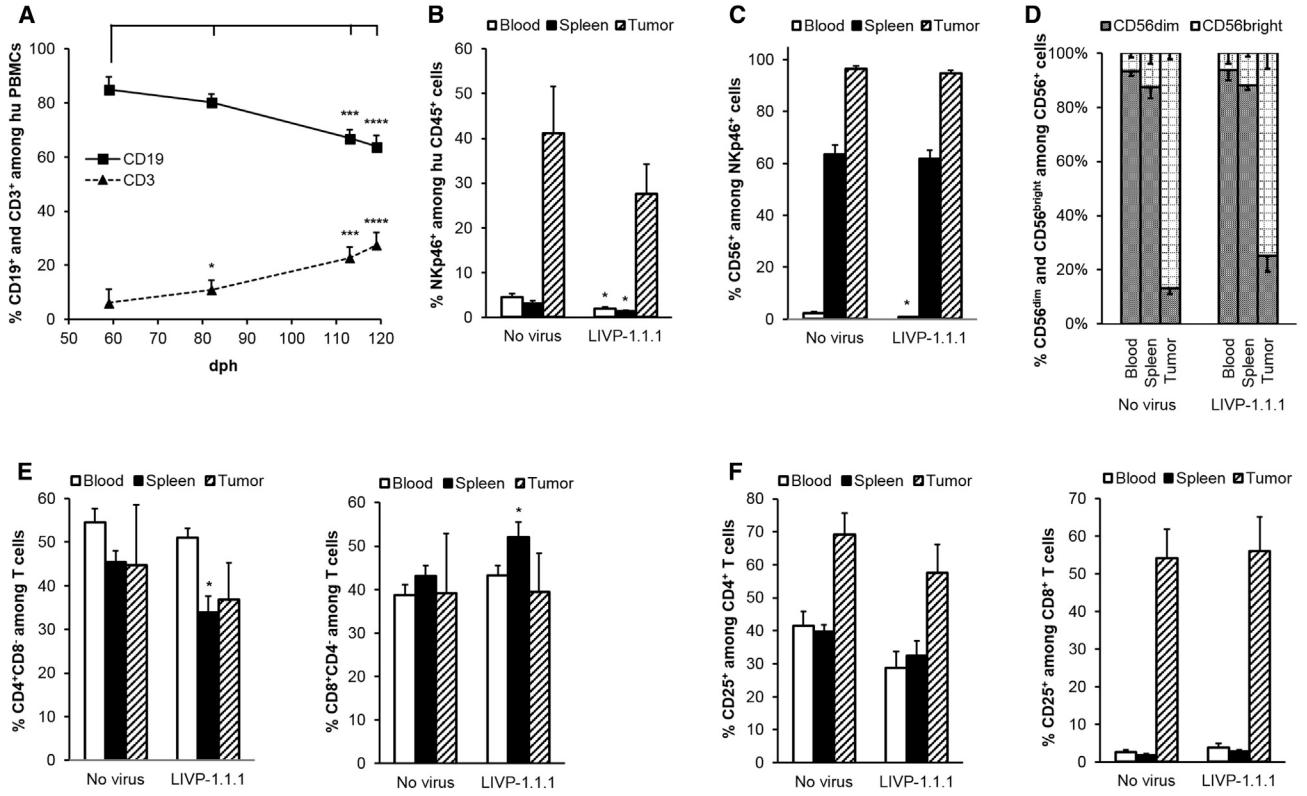

Figure 6. Flow Cytometric Analysis of Human B, T, and NK Cell Populations in Untreated or LIVP-1.1.1-Virus-Treated Tumor-Bearing Humanized NSG Mice

Human hematopoietic cells were stained with mouse anti-human monoclonal antibodies (mAbs) and gated first on human CD45 and then the respective lineage-specific marker. Flow cytometric analysis was performed, and percentages were calculated. Mean values and SEM are plotted. (A) Peripheral human $CD19^+$ B (squares) and $CD3^+$ T (triangles) cell reconstitution. Blood from humanized A549-tumor-bearing NSG mice (n = 17) was collected at 59, 82, 113, and 119 days post-humanization (dph). Gating strategy was as follows: $CD45^+ \rightarrow CD19^+$ or $CD3^+$. Differences between first and each consecutive measurement for B or T cells were tested using a two-tailed paired t test (*p < 0.05, **p < 0.01, ***p < 0.001, ****p < 0.0001). (B–F) Blood (no fill), spleen (solid fill), and tumor (diagonal) samples from untreated (n = 5) or LIVP-1.1.1-virus-injected (n = 9) A549-tumor-bearing humanized NSG mice were analyzed for presence of human immune cell reconstitution at 18 weeks post-humanization and 8 days after virus administration. Differences between corresponding samples of untreated and virus-treated groups were tested using a two-tailed t test for two samples with unequal variance (*p < 0.05, **p < 0.01, ***p < 0.001, ****p < 0.0001). (B) NK cells were gated on the NKp46 marker. (C) $CD3^-NKp46^+$ subset was additionally examined for CD56 expression. (D) Percentage of $CD56^{dim}$ (gray pattern) and $CD56^{bright}$ (dotted grid) among $CD3^-NKp46^+CD56^+$ NK cells from (C). Gating strategy was as follows: $CD45^+ \rightarrow CD3^-NKp46^+ \rightarrow CD56^+ \rightarrow (CD56^{dim}$ or $CD56^{bright})$. (E) T cells were gated on CD3 and then the respective CD4 (left panel) or CD8 (right panel) lineage-specific marker. One mouse from each group did not show tumor infiltration with T cells and was therefore excluded from the analysis of the tumor data. (F) CD4 (left panel) and CD8 (right panel) single-positive cells were additionally examined for CD25 expression. Gating strategy was as follows: $CD45^+ \rightarrow CD3^+ \rightarrow (CD4^+CD8^-$ or $CD8^+CD4^-) \rightarrow CD25^+$.

virus administration were analyzed for human B, T, and NK cell reconstitution by flow cytometry.

Highest percentages of $CD19^+$ B cells were observed in spleens (49.93% ± 6.53%, 56.64% ± 9.26%, and 54.77% ± 6.12%) of the humanized mice, where B cells represented the main immune cell subset among the human $CD45^+$ cells, followed by blood (33.13% ± 7.39%, 40.46% ± 10.12%, and 39.00% ± 7.08%), whereas very few $CD19^+$ B cells were found in tumors (2.74% ± 1.23%, 4.86% ± 2.51%, and 4.35% ± 2.46%) of untreated, GLV-1h68, and GLV-1h376 mouse groups, respectively (Figure 7A). In contrast, we found $CD3^+$ T cells to represent the main human $CD45^+$ cell population in tumors (41.36% ± 20.94%, 39.52% ± 18.13%, and 56.62% ± 13.60%), followed by blood (39.27% ± 12.19%, 39.52% ± 13.34%, and 39.84% ± 8.58%), and the lowest percentages of T cells were found in spleens (28.32% ± 7.23%, 26.31% ± 11.57%, and 27.34% ± 8.24%) of the three mouse groups (Figure 7B). Although virus treatment did not significantly change the overall B and T cell percentage in the tested organs, slightly more T cells were observed among the tumor-infiltrating human $CD45^+$ cells in the GLV-1h376 group, compared to untreated tumors. $CD4^+$ cells were the main subset among PBMC- (54.18% ± 5.34%, 54.86% ± 2.53%, and 51.26% ± 4.18%) and splenocyte- (53.85% ± 3.62%, 44.35% ± 6.74%, and 45.95% ± 5.98%) derived human T cells in untreated, GLV-1h68, and GLV-1h376 groups, respectively (Figure 7C). Lower percentages of those cells were detected among the tumor-infiltrating T cells (23.49% ± 5.37%, 14.42% ± 6.59%, and 24.87% ± 10.09%,

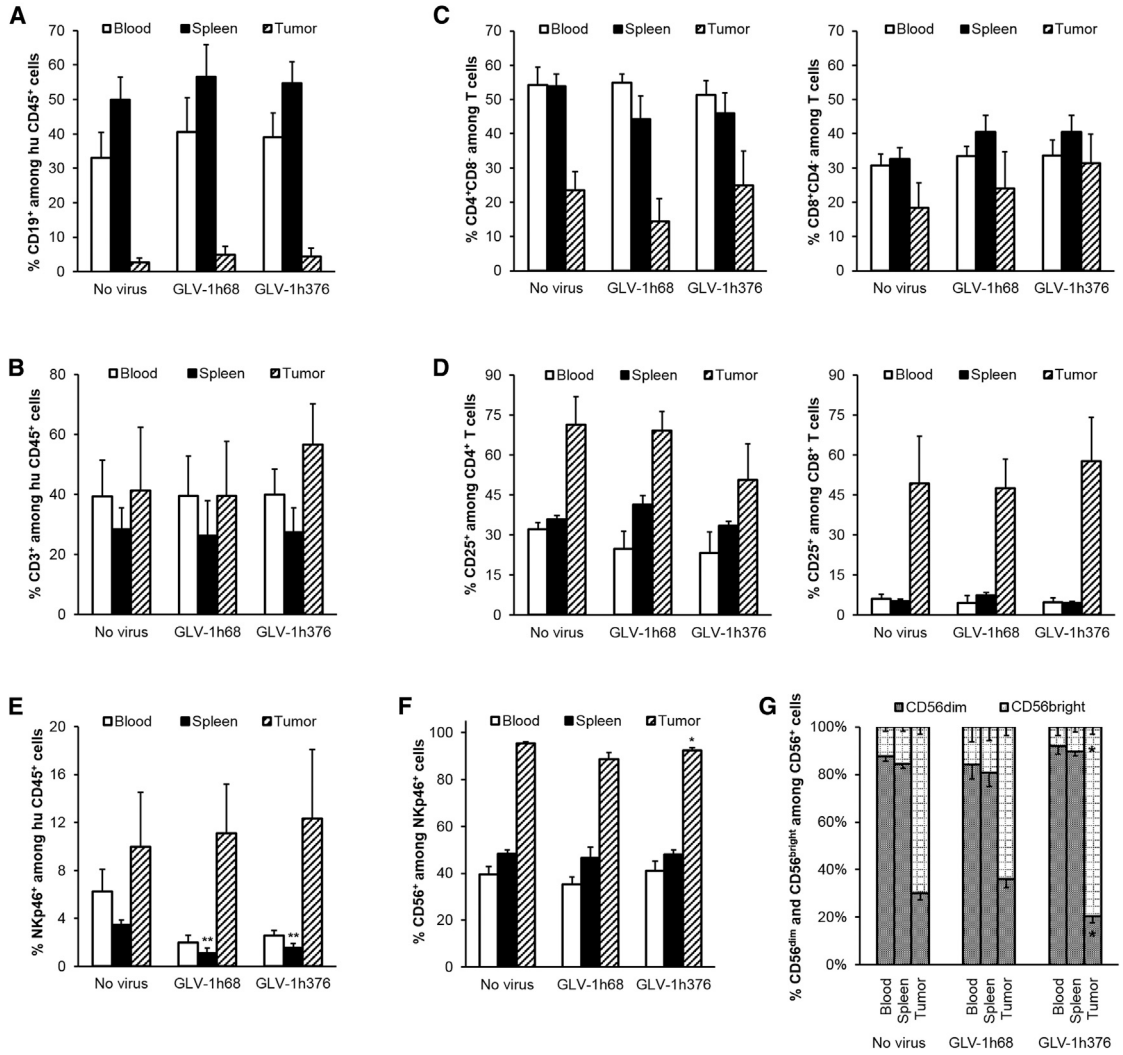

Figure 7. Presence of Human B, T, and NK Cells in Untreated and GLV-1h68- or -1h376-Injected Humanized A549-Tumor-Bearing NSG Mice

Blood (no fill), spleen (solid fill), and tumor (diagonal) samples from untreated (n = 4) or GLV-1h68- (n = 5) or -1h376- (n = 5) injected A549-tumor-bearing humanized NSG mice were analyzed by flow cytometry for presence of human immune cell reconstitution. Analysis was performed 15 weeks post-humanization and 10 days after virus administration. Human hematopoietic cells were stained with mAbs. B (A), T (B), and NK (E) cells were first gated on human CD45 and then the respective lineage-specific marker: CD19, CD3, and NKp46, respectively. (C) CD4 (left panel) or CD8 (right panel) expression was determined following gating on $CD3^+$ T cells. (D) CD4 (left panel) and CD8 (right panel) single-positive cells were additionally examined for CD25 expression. Gating strategy was as follows: $CD45^+ \rightarrow CD3^+ \rightarrow (CD4^+CD8^- \text{ or } CD8^+CD4^-) \rightarrow CD25^+$. (F) $CD3^-NKp46^+$ subset was further examined for CD56 expression. (G) Percentage of $CD56^{dim}$ (gray pattern) and $CD56^{bright}$ (dotted grid) among $CD3^-NKp46^+$ $CD56^+$ NK cells from (F). Gating strategy was as follows: $CD45^+ \rightarrow CD3^-NKp46^+ \rightarrow CD56^+ \rightarrow (CD56^{dim} \text{ or } CD56^{bright})$. Mean values and SEM are plotted. Differences between corresponding samples of untreated and virus-treated groups were tested using a two-tailed t test for two samples with unequal variance (*$p < 0.05$, **$p < 0.01$, ***$p < 0.001$, ****$p < 0.0001$).

respectively). $CD8^+$ T cells were detected in close percentage in blood (30.73% ± 3.31%, 33.53% ± 2.83%, and 33.63% ± 4.50%), spleens (32.62% ± 3.26%, 40.53% ± 4.88%, and 40.51% ± 4.91%), and tumors (18.41% ± 7.27%, 23.97% ± 10.74%, and 31.39% ± 8.47%) of the three mouse groups. Although virus treatment did not significantly change the overall percentage of both T cell subsets in the tested organs, slightly more $CD8^+$ T cells were observed among the tumor-infiltrating human $CD45^+$ cells in the GLV-1h376 group, compared to control tumors. Further analysis revealed that 32.03% ± 2.60%, 24.88% ± 6.46%, and 23.35% ± 7.82% of the $CD4^+$ T cells in blood and 35.90% ± 1.40%, 41.42% ± 3.42%, and 33.38% ± 1.61% of them in spleens of untreated, GLV-1h68-, and -1h376-treated mice, respectively, were expressing CD25 (Figure 7D). Higher percentages of $CD4^+CD25^+$ T cells were detected in tumors: 71.34% ± 10.48%, 69.17% ± 7.10%, and 50.52% ± 13.73%. Evaluation of the $CD8^+$ T cells revealed that only less than 8% of those cells were activated in blood and spleens of all three mouse

groups. In contrast, a strong activation of the cytotoxic T cells was detected in the tumor samples (49.33% ± 17.63%, 47.49% ± 10.86%, and 57.56% ± 16.62%). Although virus treatment did not significantly change the CD25 expression in tumors, slightly lower percentage of $CD4^+CD25^+$ T cells and simultaneously slightly higher levels of activated cytotoxic $CD8^+$ T cells were detected in GLV-1h376-treated tumors.

The second largest population of tumor-infiltrating human $CD45^+$ cells after the T cells were the $NKp46^+$ NK cells (Figure 7E). The highest value of 12.34% ± 5.75% was observed in GLV-1h376-infected tumors, followed by 11.11% ± 4.07% and 9.95% ± 4.55% for GLV-1h68 and untreated groups, respectively. In contrast, less than 6% and 4% of the human hematopoietic cells in blood and spleen, respectively, were NKp46 positive. Further subset analysis revealed that 95.49% ± 0.48%, 88.74% ± 2.87%, and 92.46% ± 1.17% of the $NKp46^+$ cells in tumors of untreated, GLV-1h68, and -1h376-treated mice, respectively, expressed CD56 (Figure 7F). $NKp46^+CD56^+$ NK cells were detected in close percentage in blood (39.61% ± 3.28%, 35.28% ± 3.19%, and 40.95% ± 4.12%) and spleens (48.33% ± 1.60%, 46.57% ± 4.69%, and 48.10% ± 1.76%) of the three mouse groups.

The majority of the DP $NKp46^+CD56^+$ NK cells in blood (87.57% ± 1.87%, 84.19% ± 6.14%, and 91.95% ± 3.51%) and spleens (84.55% ± 1.88%, 80.66% ± 5.71%, and 89.74% ± 2.01%) of the untreated, GLV-1h68, and GLV-1h376 mouse groups, respectively, were $CD56^{dim}$, and only a very small portion of them were $CD56^{bright}$ (Figure 7G). In contrast, most of the human $NKp46^+CD56^+$ NK cells in tumors were $CD56^{bright}$. Unlike the GLV-1h68 treatment (64.07% ± 3.51%), which did not significantly change the overall $CD56^{bright}$ percentage in tumors, compared to untreated controls (69.83% ± 2.96%), significantly ($p < 0.05$) more $CD56^{bright}$ cells among the tumor-infiltrating human $NKp46^+CD56^+$ NK cells were detected in the GLV-1h376 group (79.50% ± 2.93%).

Splenocyte-Derived Human T Cells Were Successfully Activated with Human T Cell Activation Beads Ex Vivo

Human T cells among splenocytes from untreated and GLV-1h68- or -1h376-injected humanized A549-tumor-bearing mice at 15 weeks post-humanization and 10 days after virus administration were evaluated for their ability to be activated by T cell activation beads and to recognize cell-culture-derived A549 tumor cells ex vivo.

After 48 hr in culture, the expression of the late activation marker CD25 on the T cell surface was analyzed by flow cytometry (Figure 8A). Humanized-mouse-derived T cells could successfully be activated with commercially available beads designed to mimic human dendritic cells and to specifically activate human T cells. As a result, significantly increased CD25 expression on $CD4^+$ (69.21% ± 12.20%, $p < 0.05$, $n = 3$ and 78.70% ± 8.63%, $p < 0.001$, $n = 4$) and $CD8^+$ (95.32% ± 1.44%, $p < 0.001$, $n = 3$ and 95.29% ± 3.16%, $p < 0.0001$, $n = 4$) T cells were detected for the GLV-1h68- and -1h376-treated mouse groups, respectively, compared to the control cells (9.70% ± 3.74% and 10.71% ± 3.43% for $CD4^+$ T cells and 4.73% ± 1.11% and 3.68% ± 1.00% for $CD8^+$ T cells, respectively) when no activation beads were added. Although a substantial increase in CD25 expression was also detected in bead-activated $CD4^+$ (41.09% ± 5.93%, $p < 0.05$, $n = 2$) and $CD8^+$ (81.21% ± 12.08%, $p < 0.05$, $n = 2$) T cells delivered from untreated mice, no significant difference is shown compared to mock-activated control cells (8.82% ± 1.02% and 6.08% ± 1.84%, respectively), because of the small number of mice ($n = 2$) tested in the untreated mouse group. Beside the upregulated CD25 surface marker expression, flow cytometric analyses of the splenocyte-derived T cells after treatment with activation beads showed increased intracellular human interferon-gamma (IFN-γ) synthesis (Figure 8B). A significant increase was measured in $CD4^+$ T cells from all three groups as well as among the $CD8^+$ T cells derived from untreated or GLV-1h376 mouse groups. For both T cell subsets, the highest values of 32.80% ± 4.34% and 56.96% ± 3.98%, respectively, were found in the CTLA4-expressing GLV-1h376 group. Notably, $CD4^+$ as well as $CD8^+$ T cells delivered from GLV-1h376-treated mice always showed more significant increase of the tested CD25 and INF-γ markers. Although the number of IFN-γ-expressing cells among bead-activated $CD8^+$ T cells in the GLV-1h68 group also increased substantially (30.67% ± 15.01%), there was no statistically significant difference with the control cells (1.22% ± 0.35%). In contrast to the activation with beads, incubation with A549 cells did not significantly increase either the CD25 expression or the IFN-γ synthesis on/in $CD4^+$ and $CD8^+$ T cells from any of the three mouse groups over the baseline level in the control samples.

Additionally, IFN-γ as well as interleukin-2 (IL-2) levels in collected culture supernatants from the analyzed splenocytes were measured by ELISA (Figure 8C). Substantially elevated cytokine levels were observed in all three groups after activation with beads. However, significant increase was detected only in the GLV-1h376 (89.25 ± 37.76 ng/mL, $p < 0.05$, $n = 5$, for IFN-γ and 10.72 ± 2.80 ng/mL, $p < 0.01$, $n = 5$, for IL-2) and the control (7.39 ± 0.94 ng/mL, $p < 0.01$, $n = 3$, for IL-2) groups. The most prominent increase in IFN-γ and IL-2 levels was observed in the GLV-1h376 group. The incubation of the splenocytes with A549 cells did not significantly increase cytokines amounts in any of the tested samples.

DISCUSSION

The recent FDA approval of Imlygic (Talimogene laherparepvec, T-VEC)[40] and the extensive development of other oncolytic viruses in clinical trials highlight the promise of this novel class of anti-cancer agents. However, the oncolytic-virus-elicited clinical responses are highly variable, signifying the need for further studies on the mechanisms of these responses and especially on the dynamic interactions between the malignant cells and the tumor microenvironment. Therefore, new animal models scrutinizing the effects of the oncolytic viruses on the tumor cells as well as on creating favorable microenvironment for induction of optimal anti-tumor immune responses are urgently needed. In this study, we developed a humanized subcutaneous

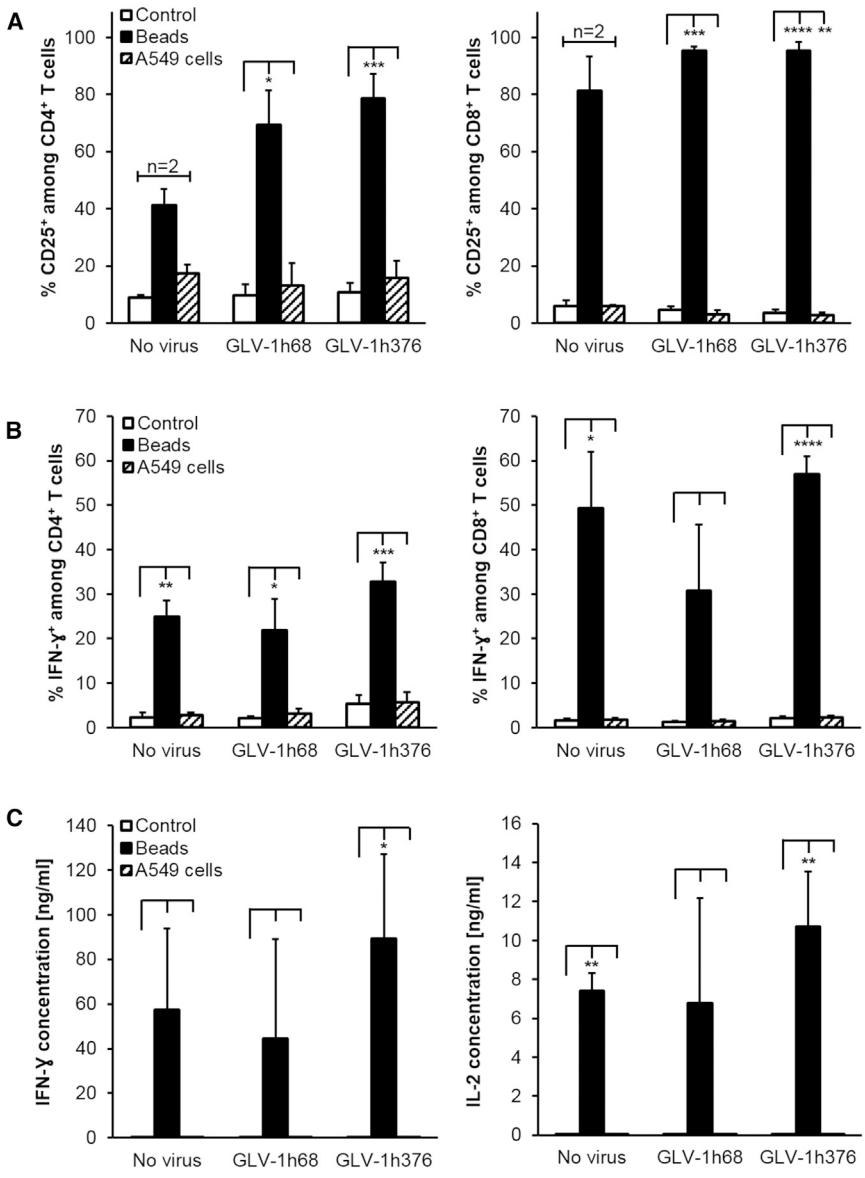

Figure 8. Splenocytes Activation Assay

Spleens from untreated, GLV-1h68-, or -1h376-injected A549-tumor-bearing humanized NSG mice were collected at 15 weeks post-humanization and 10 days after VACV administration. Single-cell suspension from each spleen was separated into three groups (equal number of cells per well) and treated with PBS (no fill), human T cell activation beads (solid fill), or irradiated A549 cells (pattern fill) for 48 hr. Differences between bead-activated or A549 cells-treated and corresponding control samples were tested using a one- or two-tailed paired t test, respectively (*$p < 0.05$, **$p < 0.01$, ***$p < 0.001$, ****$p < 0.0001$). (A) Cells were stained with mAbs against surface markers and subjected to flow cytometric analysis. CD25-expressing $CD4^+$ (left panel) and $CD8^+$ (right panel) subpopulations were first gated on human CD45 and then the respective lineage-specific marker. Gating strategy was as follows: $CD45^+ \rightarrow CD3^+ \rightarrow (CD4^+$ or $CD8^+) \rightarrow CD25^+$. Mean values in percentage and SEM of untreated (n = 2), GLV-1h68 (n = 3), and GLV-1h376 (n = 4) groups are plotted. (B) IFN-γ expression in $CD4^+$ (left panel) and $CD8^+$ (right panel) T cells was determined by intracellular staining using a mouse anti-human IFN-γ mAb. Gating strategy was as follows: $CD45^+ \rightarrow CD3^+ \rightarrow (CD4^+$ or $CD8^+) \rightarrow$ IFN-γ^+. Mean values in percentage and SEM for untreated (n = 3), GLV-1h68 (n = 4), and GLV-1h376 (n = 5) groups are plotted. (C) Human IFN-γ (left panel) and interleukin-2 (IL-2, right panel) levels in splenocytes' culture supernatant samples were assayed by ELISA. Mean values are in nanograms per milliliter, and SEM for untreated (n = 3), GLV-1h68 (n = 4), and GLV-1h376 (n = 5) groups are plotted.

tumor-bearing mouse model to study the vaccinia-virus-mediated oncolytic virotherapy and checkpoint inhibition in the context of the human immune system.

The VACV has many characteristics desirable in an oncolytic virus for clinical applications: (1) it has short, well-characterized life cycle, spreading very rapidly from cell to cell; (2) it is highly cytolytic for a broad range of tumor cell types; (3) it has a large insertion capacity (>25 kb) for the expression of exogenous genes; (4) it has high genetic stability; (5) it is amenable to large-scale production of high levels of infectious virus; (6) it does not have a known natural host and does not cause any known diseases in humans; (7) it remains in the cytoplasm and does not enter the host cell nucleus during the entire life cycle and thus does not integrate into the host genome; and (8) it has a long and established safety record in its widespread historical use in humans as a vaccine for smallpox.[41]

We report here several key findings on the development of an animal model for testing oncolytic virus potential in cancer therapy under human like conditions. First, we demonstrated the successful subcutaneous implantation of human A549 tumor cells in human-cord-blood-derived $CD34^+$ hematopoietic stem cell-engrafted NSG mice, 9–13 weeks post-humanization. Second, we analyzed the human immune system response to oncolytic VACV in the humanized mouse model with subcutaneous tumors. Third, we tested a new human CTLA4-blocking antibody-encoding GLV-1h376 VACV strain in this humanized tumor mouse model.

Successful in vivo tumor targeting after systemic administration of the GLV-2b372 VACV strain was demonstrated in the humanized subcutaneous tumor-bearing mice. The virus selectively infected and replicated in the tumors, resulting in TurboFP635 expression with 22-fold increase of fluorescent signal in tumors during the first 8 days of the infection, followed by signal decline, suggesting efficient tumor cell

lysis. Importantly, immunohistochemical analyses of GLV-2b372-infected tumors revealed that virtually the whole tumor sections were positive for VACV 15 dpi. At that late time point, the majority of tumor cells were lysed, and extensive necrotic regions and lesions were observed, explaining the decreased TurboFP635-mediated fluorescent signal.

Interestingly, in tumors of both non-humanized and humanized mice not treated with VACV, we observed multiple blood vessels and hemorrhagic regions. This finding was in line with previous reports that growing tumors are able to induce and sustain angiogenesis, via activation of an "angiogenic switch".[42,43] In contrast, the majority of tumors excised from VACV-treated humanized mice had a more compact structure with very few to no visible blood vessels. This result was expected, due to the fact that many oncolytic viruses can target, infect, and destroy developing and established tumor vasculature without harming normal blood vessels of the host.[44] More specifically, VACV targets CD31 positive tumor endothelial cells and thus reduces the blood vessel density, which together with the direct tumor cell lysis ultimately leads to the virus-mediated eradication of the tumor.

The intrahepatic transplantation of preconditioned newborn NSG mice with human-cord-blood-derived $CD34^+$ hematopoietic stem cells resulted in a successful systemic reconstitution with human immune cells. At early time points after engraftment, the majority of the human hematopoietic cells detected in the mouse blood were $CD19^+$ B cells, but with time a significant change in $CD19^+$/$CD3^+$ ratio in favor of the $CD3^+$ T cells was noted. These results suggested that for experiments focusing on the T cell population (e.g., studying the effect of the VACV-encoded anti-human CTLA4 scAb) it would be preferable to use mice that are at least 10 weeks post-humanization. Interestingly, in contrast to the blood and spleen samples, where B cells were a large or even a predominant immune cell subset, almost no B but plenty of T and NK cells were detected in tumors. Increased NK cell levels among tumor-infiltrating human $CD45^+$ cells were expected because NK cells are part of the innate immune system serving as a first-line defense against malignant and virus-infected cells.[38,45–47] However, presence of virus in the LIVP-1.1.1-infected tumors did not additionally increase the NK cell levels. As the increased numbers of tumor-infiltrating NK cells and the increased proportion of $CD56^{bright}$ cells among those NK cells were observed not only in the VACV-infected, but also in the non-treated tumors, the implanted human A549 tumor cells but not the subsequent viral infection of those tumors are the likely reason for this NK cell accumulation. Unlike a previous report,[26] where tumor cells were implanted together with the human-cord-blood-derived $CD34^+$ hematopoietic stem cells into newborn NSG mice to avoid allograft rejection of eventually HLA-mismatched human tumor cells, in the present humanized tumor mouse model, the tumor cells were implanted at least 9 weeks following humanization. Therefore, already developed human immune cells could potentially target the A549 tumors. However, the implanted tumor cells were still able to form tumors, suggesting deficiencies of the human immune system in the humanized mice.

NK cells have already been shown to be able to promote allograft tolerance.[48–50] More interestingly, a high number of NK cells in the uterine endometrium expressing almost exclusively $CD56^{bright}$ and producing IL-4 and IL-10 have been shown to play an important role in trophoblast invasion, development of placenta, angiogenesis, and maintenance of the early pregnancy.[51–54] Immunoregulatory $CD56^{bright}$ cells, able to downregulate the immune responses and reduce inflammation by producing the immunosuppressive cytokine IL-10, were observed also in context of different diseases.[52] Therefore, we believe that the large percentage of $CD56^{bright}$ cells found in the tumors of the humanized mice were regulatory NK cells, able to deliver immunosuppressive cytokines and to alter the T cell responses allowing the A549 tumor development.

We found that approximately half of the tumor-infiltrating human T cells were $CD4^+$ and the other half were $CD8^+$, with the majority of them expressing CD25. Interestingly, less than 7% of the $CD8^+$ T cells in blood and spleens were expressing CD25, in contrast to the tumors, where at least 47% of the $CD8^+$ T cells expressed the marker. Nevertheless, the greatest activation of the tumor-infiltrating effector lymphocytes was again not caused by the virus, as these cells expressed CD25 even in the absence of virus. However, despite the presence of activated cytotoxic T cells in the tumors, a progressive tumor growth was observed after the subcutaneous A549 cancer cell implantation.

The combination therapy with oncolytic viruses and immune checkpoint inhibitors is currently under active clinical investigation. The combined use of the first FDA-approved oncolytic virus T-VEC with Ipilimumab (NCT01740297) or with Pembrolizumab (NCT02263508) is being evaluated in clinical trials for metastatic melanoma. Primary analysis of the phase Ib study of T-VEC plus Ipilimumab is very promising, with significantly better objective responses, suggesting an improvement in efficacy of combination therapy as compared to the single treatment.[55]

Not systemic but locoregional administration of the immunomodulatory antibodies to the tumor site may be the most effective approach to induce antitumor immunity. Our recent work using VACV combined with intratumoral CTLA4 blockade in a syngeneic murine lymphoma model was the first to demonstrate the potential of combination immunotherapy with oncolytic viruses and checkpoint inhibitors in hematologic malignancies.[56] The observed antitumor activity was attributed to the induction of an effective and specific immune response. This finding was corroborated by the significant infiltration with mature activated NK cells, followed by $CD8^+$ T cells, in both treated and untreated tumors. Importantly, the tumor-specific $CD8^+$ T cells showing a memory phenotype ($CD44^{hi}$) suggested the effective induction of a potent immune memory response. Effective targeting of distant metastases after intratumoral administration of both VACV and CTLA4-blocking antibody was also an important finding with significant clinical implications. Intratumoral administration of significantly lower doses of immunomodulatory antibodies such as anti-CTLA4 and anti-OX40 was reported by Marabelle et al.

as equally effective to systemic treatment, with antitumor efficacy seen at distant sites.[57] Zamarin et al. reported effective combination therapy with intratumoral oncolytic virus application and systemic CTLA4 blockade leading to rejection of distant tumors and protection from tumor re-challenge in poorly immunogenic tumor models.[58] The observed therapeutic effect was associated with inflammatory immune infiltrates in distant tumors, making them susceptible to systemic therapy with immunomodulatory antibodies.

These findings suggest that expression of immunomodulatory antibody at the tumor site by genetically engineered oncolytic viruses may prove to be the most effective in eliciting antitumor immunity. Additionally, we proposed that a replacement of the monoclonal antibody used in the clinic with a smaller single-chain antibody could improve its distribution within the tumors. Therefore, in this study we used a new recombinant GLV-1h376 VACV encoding human CTLA4-blocking single-chain antibody to evaluate whether CTLA4 immune checkpoint blockade could enhance the induction of antitumor immunity. Before its application in humanized mice, we demonstrated the ability of the newly constructed VACV to infect, replicate in, and kill different cancer cell lines in a time-dependent fashion. Further, the GLV-1h376-encoded CTLA4 scAb was successfully secreted from infected cells and purified. This allowed us to prove its human specificity in vitro and functionality in cell culture. Surprisingly, in spite of the successful tumor colonization following systemic administration of GLV-1h376 resulting in a significant increase of the $CD56^{bright}$ NK cell subset, this virus was not able to increase cytotoxic T or overall NK cell levels at the tumor site.

Splenocyte-derived human T cells from untreated and GLV-1h68- or -1h376-treated humanized tumor-bearing mice were functional and could successfully be activated with commercially available beads designed to mimic human dendritic cells. As a result, increased CD25 expression and intracellular IFN-ɣ production among $CD4^+$ and $CD8^+$ T cells along with increased IL-2 and IFN-ɣ release were observed. Interestingly, $CD4^+$ as well as $CD8^+$ T cells delivered from GLV-1h376-treated mice always showed more prominent increase of the tested markers, suggesting that these cells might have been pre-activated due to the CTLA4 blockade by the virus-encoded CTLA4 scAb in the GLV-1h376-treated mice. In contrast to the activation with beads, T cells from all three mouse groups were not able to recognize and to be activated by A549 tumor cells. A possible explanation for the lack of activation could be that very little to no tumor-specific T cells were residing in the spleens. As no increase in activation markers was detected, a more plausible explanation could be that T cells were not exposed to tumor-associated antigens due to missing or dysfunctional antigen-presenting cells in the humanized mouse model. This assumption was supported by a previous report[59] showing that although few myeloid cells could be found in the circulation of such humanized mice[60] they are phenotypically immature and functionally impaired.[61] Other reasons as an explanation for unresponsiveness could be a weak immunogenicity of the used tumor[62] or not enough time given for the maturation of the naive immune system of the humanized mice and/or the short interval for measurement after VACV treatment of the mice.[63,64]

Beside the CTLA4 scAb expression cassette, GLV-1h376 also carries the *E. coli* β-glucuronidase-encoding (*gusA*) gene. The quantitative β-glucuronidase assay using this GusA enzyme is a very promising and well established in our laboratory reporter system.[27–29] It is very accurate, requires very small sample volume, uses inexpensive substrates, and could be carried out in a very short time. Importantly, excellent correlations between levels of CTLA4 scAb, GusA, and viral titers, assayed separately by ELISA, β-glucuronidase assay, and standard plaque assay, respectively, in A549 cultures and humanized-mouse-derived human A549 tumors infected with GLV-1h376 were observed. These results indicate that each of the three parameters could be used to estimate the amount of the other two and, more importantly, that β-glucuronidase assay, which is the least time and sample consuming as well as the least labor intensive of the three assays, would be sufficient to perform to test viral titers, GusA, and CTLA4 scAb concentrations in humanized-mouse-derived tumor samples after treatment with GLV-1h376.

In conclusion, we established a humanized tumor mouse model and characterized the functionality and potential of a CTLA4-blocking antibody/oncolytic VACV combination therapy. Further studies using more immunogenic tumors in combination with increased treatment intervals need to be performed to further evaluate the efficacy of this therapy and to optimize the capability of this humanized tumor mouse model. However, humanized mouse models allow the characterization of positive and negative effects of treatment approaches in interaction with the human immune system prior to clinical testing.

MATERIALS AND METHODS

Cell Culture

The A549 (human lung carcinoma, CRM-CCL-185) and the CV-1 (African green monkey kidney fibroblasts, CCL-70) cells were obtained from the American Type Culture Collection (ATCC). A549 cells were cultured in RPMI 1640 supplemented with 10% FBS under standard cell-culture conditions (37°C, 5% CO_2, and over 95% humidity). CV-1 cells were cultured in DMEM instead of RPMI 1640. The 1935-MEL and 888-MEL melanoma cell lines were kindly provided by A.G. Szalay (Biocenter, University of Wuerzburg) and cultured in RPMI 1640 supplemented with 1 mM sodium pyruvate, 1 × MEM nonessential amino acids solution, and 10% fetal bovine serum (FBS). All media and supplements were obtained from Mediatech.

VACV Strains

The WT LIVP VACV stain, which was used as a vaccine and originate from the Lister strain, was the parental strain for all viruses used. LIVP-1.1.1 is an isolate from the WT LIVP with naturally disrupted *J2R* locus.

Standard cloning techniques were used for the construction of the plasmids for the generation of the recombinant VACV strains. The cDNA encoding for TurboFP635 was PCR amplified using

plasmid FUKW (kindly provided by Dr. Marco J. Herold, University of Wuerzburg) as a template with primers FUKW-5 (5′-GTCGAC (SalI) CACCATGGTGGGTGAGGATAGCGTGC-3′) and FUKW-3 (5′-TTAATTAA(Pac I) TCAGCTGTGCCCCAGTTTGC-3′). The PCR product was gel purified and cloned into the pCR-Blunt II-TOPO vector using Zero Blunt TOPO PCR Cloning Kit (Invitrogen). The resulting construct pCRII-FUKW was sequence confirmed. The TurboFP635 cDNA was then released from pCRII-FUKW with SalI and *Pac*I and sub-cloned into TK-SEL-hNISa8 with the same cuts by replacing hNIS cDNA. The gpt selection-expression cassette was located outside the VACV DNA that directs homologous recombination into the TK locus of virus genome, allowing for transient dominant selection of vaccinia recombinants.[65] The resulting construct TK-SEL-FUKW1 was sequence confirmed and used to make the recombinant GLV-2b372 virus from the parental LIVP-1.1.1 virus.

The highly attenuated oncolytic recombinant VACV GLV-1h68 was previously described by Zhang et al.[10] In brief, this triple mutant was constructed by insertion of *Renilla* luciferase-*Aequorea* GFP fusion (*ruc-gfp*), β-galactosidase (*TrfR lacZ*), and *E. coli* β-glucuronidase (*gusA*) expression cassettes into the *F14.5L*, *J2R*, and *A56R* loci and under the control of VACV synthetic early/late (P_{SEL}), VACV 7.5K early/late ($P_{7.5}$), and VACV late (P_{11}) promoter, respectively.

Regarding the CTLA4 scAb-encoding GLV-1h375, -1h376, and -1h377 viruses, the open reading frame (ORF) for the CTLA4 scAb was synthesized and cloned into the plasmid pUC57 by GenScript. The plasmid contains a fragment coding for the single-chain fragment variable CTLA4 scAb, comprising a Igκ light chain leader sequence,[66] the V_H chain sequence of the antibody clone 11.2.1,[67] a $(G_4S)_3$ linker sequence, the V_L chain sequence of the antibody clone 11.2.1, and a C-terminal DDDDK sequence. To construct the final plasmids, the VACV DNA homology-based shuttle plasmids pCR-TK-P_{SE}, pCR-TK-P_{SEL}, and pCR-TK-P_{SL} (Q. Zhang, unpublished data) were used. The *anti-CTLA4* fragment was cloned into the framework of the plasmids via the SalI and *Pac*I sites, resulting in the plasmids pCR-TK-P_{SE}-*anti-CTLA4*, pCR-TK-P_{SEL}-*anti-CTLA4*, and pCR-TK-P_{SL}-*anti-CTLA4*. The recombinant viruses GLV-1h375, -1h376, and -1h377 were constructed as previously described.[65] The three viruses contain the *anti-CTLA4* gene under the control of the VACV synthetic early (P_{SE}), early/late (P_{SEL}), and late (P_{SL}) promoters, respectively. It was inserted into the TK locus by homologous recombination and was constructed from the parental strain GLV-1h68. Recombinant viruses were propagated in CV-1 cells, and up to 2×10^9 PFUs/mL could be purified from infected CV-1 cells through sucrose gradients.[68]

Figure 1A shows a schematic overview of the VACV constructs and marker gene locations in the genome.

Viral Infection Assay

A549, 1935-MEL, and 888-MEL cells were seeded onto 24-well plates. After 18–24 hr in culture, the cells were infected with LIVP-1.1.1, GLV-2b372, -1h68, -1h375, -1h376, or -1h377 at an MOI of 0.005 or 0.1. Infection was performed using medium supplemented with 1% antibiotic-antimycotic solution (Mediatech) and 2% FBS. Plates were incubated for 1 hr at 37°C with gentle agitation every 20 min. The infection medium was then replaced with fresh growth medium without phenol red, supplemented with 1% antibiotic-antimycotic solution. At 24, 48, 72, and 96 hpi, the supernatant was removed and stored at −80°C. Fresh medium (1 mL) was added to the infected cells, which were then frozen at −80°C. After thawing, all cell fragments were mechanically removed from the plates by pipetting. All samples underwent three freeze and thaw cycles and were sonicated three times for 30 s. For viral replication assays, viral titers were determined by standard plaque assay.

Cytotoxicity Assay

To determine the cytotoxicity of LIVP-1.1.1, GLV-2b372, -1h68, -1h375, -1h376, or -1h377 on A549, 1935-MEL, and 888-MEL cells, tumor cells were seeded onto 24-well plates, cultured for 18–24 hr, and infected in triplicates at an MOI of 0.1 or mock infected. After 1 hr of incubation at 37°C under 5% CO_2, the virus-containing and mock supernatants were aspirated, and 1 mL of fresh growth medium was added to each well. At 24, 48, 72, and 96 hpi, the culture media was replaced with 500 μL of MTT (Sigma) dissolved in RPMI 1640 medium without phenol red (Mediatech) at a concentration of 2.5 mg/mL, and the plates were incubated for 2 hr at 37°C. MTT solution was then removed, and the plates were stored at −80°C. After collecting the plates from all time points, they were thawed, and 500 μL of 1 N HCL diluted in isopropanol was added to all control and test wells. Absorbance was measured in 96-well plates at 570 nm in a Spectra Max M5 microplate reader (Molecular Devices). Uninfected cells were considered as 100% viable. Cytotoxicity was calculated using the following formula: % viable cells = [OD (infected cells) / OD (uninfected cells)] × 100.

Purification and Detection of CTLA scAb

CV-1 cells were seeded in T-225 flasks and cultured at 37°C overnight. The growth medium was replaced by 15 mL of DMEM containing GLV-1h376 at an MOI of 2 for 24 hr. After removing the viral particles using a 0.1-μL syringe filter, the CTLA4 scAb-containing supernatant was concentrated by centrifugation with Amicon Ultra-15 columns (EMD Millipore). FLAG-tagged single-chain antibody was purified from the concentrate using the FLAG Immunoprecipitation Kit (Sigma). The correct molecular mass of the purified antibody was verified on Coomassie stained gel. Its concentration was measured using the DC Protein Assay Kit (Bio-Rad).

For CTLA4 scAb protein expression, A549 cells were infected with rVACV strains at an MOI of 1. Cell lysates and supernatants of infected cultures were collected 24 hr later, and 4 and 10 μg of denatured protein, respectively, were separated by SDS-PAGE, transferred to a polyvinylidene fluoride (PVDF) membrane and detected using a primary rabbit anti-DDDDK antibody (Abcam), a secondary horseradish-peroxidase-labeled anti-rabbit IgG antibody (Bio-Rad), and the Opti4CN detection kit (Bio-Rad).

The presence of CTLA4 scAb in cell-culture or mouse-derived samples was tested by ELISA assays. Ninety-six-well plates were pre-coated with rh CTLA4 Fc chimera (R&D Systems), blocked, and incubated for 1 hr at room temperature with the test samples and standard dilutions, followed by a primary rabbit anti-DDDDK antibody (Abcam) and a secondary horseradish peroxidase-labeled anti-rabbit IgG antibody (Bio-Rad). Wells were washed with PBS/0.05% Tween after each incubation step. Color was developed using 3,3′,5,5′-tetramethylbenzidine (Sigma), and the reaction was stopped by adding 2N HCl. Absorbance was measured at 450 nm in a Spectra Max M5 microplate reader (Molecular Devices). Affinity of GLV-1h376-encoded CTLA4 scAb to human CTLA4 and lack of cross-reactivity to mouse CTLA4 in vitro was tested using the same ELISA setup, but 96-well plates were pre-coated with either rh CTLA4 Fc chimera or rm CTLA4 Fc chimera, respectively, both from R&D Systems, and incubated with dilutions of purified CTLA4 scAb as test samples.

Mice

Timed-pregnant NOD.Cg-Prkdc^{scid} Il2rg^{tm1Wjl}/SzJ (NSG) mice were purchased from The Jackson Laboratory and allowed to acclimatize for 3–6 days before giving birth under pathogen-free conditions in HEPA-filtered, individually ventilated disposable cages (Innovive) with irradiated food and pre-bottled acidified water (Innovive) in the animal facilities of Explora Biolabs at the San Diego Science Center. Newborn pups were irradiated with 0.8 Gy using a RadSource RS 2000 irradiator (Rad Source Technologies). Within 3 hours of irradiation, the pups were injected into the liver with 1.8 × 105 to 3 × 105 human-cord-blood (Cryopoint)-derived CD34+ hematopoietic stem cells. Isolation of CD34$^+$ cells was performed using a CD34 MicroBead Kit (Miltenyi Biotec) according to the manufacturer's instructions. The peripheral blood collected from CD34$^+$ cell-engrafted animals was routinely evaluated for human immune cell reconstitution. Nine to 13 weeks post-transplantation, mice were implanted subcutaneously with 5×10^6 A549 cells into the right hind leg. When tumors reached an average size of 250–350 mm^3, VACV was administered systemically by retro-orbital (r.o.) inoculation of 6×10^6 PFUs in 100 μL PBS at day 0 of the infection. Mice were observed daily for any adverse effects, including signs of morbidity. All efforts were made to minimize stress. More blood and different organs were collected at the end of each experiment, when animals were sacrificed.

All animal studies were approved by and performed in strict accordance with the guidelines of the Institutional Animal Care and Use Committee of Explora Biolabs (IACUC), San Diego Science Center (approval number: EB12-018 and EB11-025).

Preparation of Single-Cell Suspensions and Mononuclear Cell Isolations

Peripheral blood was collected from the saphenous vein or the retro-orbital sinus using EDTA-coated capillary tubes (Drummond Scientific) and EDTA-treated tubes (Becton Dickinson). On the final day of the experiment, blood was collected by cardiac puncture. Erythrocytes were lysed with 1 × RBC Lysis Buffer (eBioscience), and PBMCs were washed with fluorescence-activated cell sorting (FACS) buffer (PBS supplemented with 2% FBS).

Spleens and tumors were excised, weighted, inspected, and prepared for flow cytometry analyses. Spleen tissue was homogenized between the frosted ends of microscopic slides, passed through an 18G needle, and filtered through a 70-μL cell strainer. Red blood cells were lysed as described above. Tumor tissue was cut into small pieces and placed in RPMI 1640 supplemented with 0.5 mg/mL Collagenase D (Roche Diagnostics), 0.2 mg/mL hyaluronidase type V (Sigma), 0.0015 mg/mL DNase I type IV (Sigma), and 1% FBS for 1 hr at 37°C. Tumor suspension was then filtered through a 70-μL cell strainer and washed with FACS buffer.

Tumor Homogenates

Tumors were excised, weighted, and gently disrupted into small pieces in RPMI 1640 without phenol red (Mediatech) supplemented with 2% FBS on ice and then homogenized using a MagNA Lyser Instrument (Roche Diagnostic) at 6,000 rpm for 30 s, followed by three subsequent freeze (−80°C) and thaw (37°C) cycles. Viral titer and β-glucuronidase and CTLA4 scAb concentrations were determined by standard plaque assay, β-glucuronidase assay, and ELISA, respectively.

Flow Cytometry

Reconstitution with human immune cells in different mouse organs as well as activation of splenocyte-derived T cells and Jurkat cells was assessed by multicolor flow cytometry. The following monoclonal antibodies (mAbs) were used: anti-human CD45-APC (HI30), CD19-FITC (HIB19), CD3-APC-H7 (SK7), CD4-PE (SK3), CD8-FITC and CD8-PE (HIT8a), CD25-BV421 (M-A251), CD69-PE and CD69-FITC (FN50), Nkp46-PE-Cy7 (9E2/NKp46), CD56-PE (MY31), and IFN-ɣ-PerCP-Cy5.5 (B27) from BD Biosciences. To reduce nonspecific binding, human and/or mouse BD Fc Block were used (BD Biosciences). To determine the viability of cells, samples were incubated with LIVE/DEAD Fixable Aqua Dead Cell Stain Kit (Life Technologies) according to the manufacturer's instructions. Dead cells were excluded from the analysis by gating out low forward scatter and brightly aqua fluorescent reactive dye-retaining cells. For compensations, single staining and/or AbC anti-mouse bead kit (Life Technologies) were used. To identify gating boundaries, unstained, single-stained, and/or fluorescence minus one (FMO) controls were used. Samples were acquired with a BD FACSCanto flow cytometer (BD Biosciences) at the VA hospital Flow Cytometry Core facility using established protocols. Data analysis was performed using FlowJo version 10 (FLOWJO) software.

Activation of Splenocytes

Single-cell suspension of spleens from A549-tumor-bearing humanized mice were prepared, and an equal number of suspended cells from each spleen was distributed into three groups. Untreated cells from group 1 were used as a control. The T cells from group 2 were activated using a human T Cell Activation/Expansion Kit (Miltenyi Biotec) according to the manufacturer's instructions. Next, to

assess the ability of the human immune cells to recognize and be activated by the A549 cells ex vivo, tumor cells were irradiated with 30 Gy using a Cesium-137 irradiator at the Moores UCSD Cancer Center and added to the spleen suspension of group 3 (tumor-to-immune cell ratio 1:10). All three groups were cultured in RPMI 1640 supplemented with 2 mM glutamine, 1 mM sodium pyruvate, 10 mM HEPES, 1% MEM nonessential amino acids, and 1% antibiotic-antimycotic solution, all obtained from Mediatech, as well as 10% human AB serum (GEMINI Bio-Products) under standard cell-culture conditions. Forty-eight hours later, samples from all three groups were stained for human immune cell-surface antigens, CD45, CD3, CD4, CD8, and CD25, and intracellular human IFN-ɣ. Interferon-ɣ was stained using a BD Cytofix/CytopermPlus Fixation/Permeabilization Kit with BD GolgiStop protein transport inhibitor containing monensin, following the manufacturer's instructions, and an anti-human IFN-ɣ-PerCP-Cy5.5 (B27) antibody, both from BD Biosciences. The untreated cells from control group 1 were used to set the location of gates in the following flow cytometry analysis. Interferon-ɣ and IL-2 concentrations in culture supernatants were measured using human INF-ɣ and IL-2 ELISA kits (Pierce Biotechnology).

Activation of Jurkat Cells

Two methods for activation of Jurkat cells were used. Jurkat cells were activated for 48 hr with a human T Cell Activation/Expansion Kit from Miltenyi Biotec following the manufacturer's instructions or a mixture of 0.003 μg/mL PMA (Sigma), 0.3 μg/mL ionomycin (Sigma), 0.5 μg/mL recombinant human B7-1 Fc chimera (R&D Systems), and 0.5 μg/mL recombinant human B7-2 Fc chimera (R&D Systems) (using concentrations obtained from a previous publication[69] but adapted for this experiment). Additionally, 1.2 μg/mL purified GLV-1h376-encoded CTLA4-blocking single-chain antibody was added to some of the wells. Successful activation was determined by flow cytometry.

Fluorescence Imaging

GFP and TurboFP635 expression in A549 cell cultures infected with GLV-1h68 and -2b372 at an MOI of 0.1 was imaged at 24, 48, 72, and 96 hpi using an inverted Olympus IX71 microscope with an Olympus MicroFire digital CCD camera. Whole-field brightness increase by 40% was applied equally across the entire image of all cell-culture GFP images using PowerPoint (Microsoft).

The expression of the GFP protein in GLV-1h68- and -1h376-infected A549 tumors was imaged ex vivo using a Leica M165 FC Fluorescence Classic Stereomicroscope and Leica Application Suite V3.7 from Leica Microsystems.

Tumor-bearing mice infected with GLV-2b372 were anesthetized by isoflurane inhalation and imaged for TurboFP635 expression at 3, 8, and 15 dpi using a Carestream Imager (Bruker). The obtained images and results in relative fluorescence units were processed using Molecular Imaging Software "MI" 7.1 (Bruker) for Windows and Microsoft Excel.

Beta-Glucuronidase Assay

To detect β-glucuronidase expression in cell-culture and mouse samples, 5 μL of test sample or standard solution with a known β-glucuronidase concentration was added to black 384-well optical bottom plates (Thermo Fisher Scientific). After addition of 75 μL of PBS supplemented with 2% FBS and 0.2 μL of 36.5 mM 6-Chloro-4-methylumbelliferyl β-D-glucuronide (Glycosynth) stock solution in dimethyl sulfoxide, plates were incubated for 1 hr at 37°C. Fluorescence was measured at excitation and emission wavelengths of 365 and 455 nm in a Spectra Max M5 microplate reader (Molecular Devices). Results were presented in relative fluorescent units. Serial dilutions of standard β-glucuronidase for establishing the standards curve were prepared for each measurement.

Immunohistochemistry of Paraffin Sections

Humanized and control mice were euthanized by CO_2 asphyxiation. Tissues for histopathologic examination were fixed in 10% neutral buffered formalin overnight, dehydrated through a series of increasing alcohol concentrations, and embedded in paraffin. Paraffin blocks were sectioned at 5 μm. Sections were rehydrated, and citrate buffer was used for antigen retrieval. Tissues were peroxidase treated. Immunohistochemical staining was performed using the VECTASTAIN Elite ABC Kit (Vector Laboratories) according to the manufacturer's instruction. Primary rabbit-polyclonal IgG to VACV (Abcam) was used. Suitable staining was developed with ImmPACT DAB Peroxidase Substrate (Vector Laboratories). After counterstaining with hematoxylin (Vector Laboratories) and dehydration step, slides were mounted in Richard-Allan Scientific Mounting Medium (Richard Allan Scientific).

Statistical Analysis

Statistical analyses were performed in Microsoft Excel. Mean values ± SEM were presented. Statistical differences between two groups were calculated with Student's t test. p values <0.05 were considered statistically significant. Statistical significance is indicated by asterisks as follows: *$p < 0.05$, **$p < 0.01$, ***$p < 0.001$, ****$p < 0.0001$.

SUPPLEMENTAL INFORMATION

Supplemental Information includes two figures and can be found with this article online at http://dx.doi.org/10.1016/j.omto.2017.03.001.

AUTHOR CONTRIBUTIONS

D.T., B.M., and A.A.S. designed the study. D.T., B.M., and A.K.W. developed the methodology. D.T., Q.Z., and A.F. performed experiments. D.T., B.M., and A.A.S. analyzed and interpreted the data. A.K.W. provided expertise and feedback. D.T., Q.Z., A.F., and B.M. wrote the original draft. A.A.S., A.K.W., B.M., and D.T. reviewed and edited the manuscript. A.A.S. and B.M. supervised the project. A.A.S. secured funding.

CONFLICTS OF INTEREST

No competing financial interests exist for the first author, D.T. Several of the authors (Q.Z., A.F., B.M., and A.A.S.) are/were salaried employees and/or shareholders of Genelux Corporation during this

study. The funders had no role in the study design, data collection and analysis, decision to publish, or preparation of the manuscript.

ACKNOWLEDGMENTS

This work was supported by Genelux Corporation and a graduate stipend from the University of Wuerzburg (to D.T.) and by a Research Service Grant awarded by Genelux Corporation to the University of Wuerzburg. The authors thank Nanhai Chen (Genelux Corporation) for virus preparation, Terry Trevino, Jason Aguilar, and Uma Sukhwani (Genelux Corporation) for their technical assistance. We thank Prof. Dr. Leonard D. Shultz (Jackson Laboratory) for providing access to NSG mice. The study was supported by Genelux Corporation (R&D Facility) and a Research Service Grant awarded by Genelux Corporation to the University of Wuerzburg in Germany.

REFERENCES

1. International Agency for Research on Cancer of World Health Organisation (2014). World Cancer Report 2014, B.W. Stewart and C. Wild, eds. (IARC).
2. Woo, Y., Adusumilli, P.S., and Fong, Y. (2006). Advances in oncolytic viral therapy. Curr. Opin. Investig. Drugs *7*, 549–559.
3. Mullen, J.T., and Tanabe, K.K. (2003). Viral oncolysis for malignant liver tumors. Ann. Surg. Oncol. *10*, 596–605.
4. Chen, N.G., and Szalay, A.A. (2010). Oncolytic vaccinia virus: A theranostic agent for cancer. Future Virol. *5*, 763–784.
5. Kaufman, H.L., Kohlhapp, F.J., and Zloza, A. (2015). Oncolytic viruses: A new class of immunotherapy drugs. Nat. Rev. Drug Discov. *14*, 642–662.
6. Thorne, S.H., Bartlett, D.L., and Kirn, D.H. (2005). The use of oncolytic vaccinia viruses in the treatment of cancer: A new role for an old ally? Curr. Gene Ther. *5*, 429–443.
7. Henderson, D.A. (1976). The eradication of smallpox. Sci. Am. *235*, 25–33.
8. Arita, I. (1979). Virological evidence for the success of the smallpox eradication programme. Nature *279*, 293–298.
9. Yu, Y.A., Shabahang, S., Timiryasova, T.M., Zhang, Q., Beltz, R., Gentschev, I., Goebel, W., and Szalay, A.A. (2004). Visualization of tumors and metastases in live animals with bacteria and vaccinia virus encoding light-emitting proteins. Nat. Biotechnol. *22*, 313–320.
10. Zhang, Q., Yu, Y.A., Wang, E., Chen, N., Danner, R.L., Munson, P.J., Marincola, F.M., and Szalay, A.A. (2007). Eradication of solid human breast tumors in nude mice with an intravenously injected light-emitting oncolytic vaccinia virus. Cancer Res. *67*, 10038–10046.
11. Frentzen, A., Yu, Y.A., Chen, N., Zhang, Q., Weibel, S., Raab, V., and Szalay, A.A. (2009). Anti-VEGF single-chain antibody GLAF-1 encoded by oncolytic vaccinia virus significantly enhances antitumor therapy. Proc. Natl. Acad. Sci. USA *106*, 12915–12920.
12. Donat, U., Weibel, S., Hess, M., Stritzker, J., Härtl, B., Sturm, J.B., Chen, N.G., Gentschev, I., and Szalay, A.A. (2012). Preferential colonization of metastases by oncolytic vaccinia virus strain GLV-1h68 in a human PC-3 prostate cancer model in nude mice. PLoS ONE *7*, e45942.
13. Kirn, D.H., and Thorne, S.H. (2009). Targeted and armed oncolytic poxviruses: A novel multi-mechanistic therapeutic class for cancer. Nat. Rev. Cancer *9*, 64–71.
14. Heo, J., Reid, T., Ruo, L., Breitbach, C.J., Rose, S., Bloomston, M., Cho, M., Lim, H.Y., Chung, H.C., Kim, C.W., et al. (2013). Randomized dose-finding clinical trial of oncolytic immunotherapeutic vaccinia JX-594 in liver cancer. Nat. Med. *19*, 329–336.
15. Mestas, J., and Hughes, C.C. (2004). Of mice and not men: Differences between mouse and human immunology. J. Immunol. *172*, 2731–2738.
16. McCune, J.M., Namikawa, R., Kaneshima, H., Shultz, L.D., Lieberman, M., and Weissman, I.L. (1988). The SCID-hu mouse: Murine model for the analysis of human hematolymphoid differentiation and function. Science *241*, 1632–1639.
17. Bosma, G.C., Custer, R.P., and Bosma, M.J. (1983). A severe combined immunodeficiency mutation in the mouse. Nature *301*, 527–530.
18. Vormoor, J., Lapidot, T., Pflumio, F., Risdon, G., Patterson, B., Broxmeyer, H.E., and Dick, J.E. (1994). Immature human cord blood progenitors engraft and proliferate to high levels in severe combined immunodeficient mice. Blood *83*, 2489–2497.
19. Prochazka, M., Gaskins, H.R., Shultz, L.D., and Leiter, E.H. (1992). The nonobese diabetic scid mouse: Model for spontaneous thymomagenesis associated with immunodeficiency. Proc. Natl. Acad. Sci. USA *89*, 3290–3294.
20. Shultz, L.D., Schweitzer, P.A., Christianson, S.W., Gott, B., Schweitzer, I.B., Tennent, B., McKenna, S., Mobraaten, L., Rajan, T.V., Greiner, D.L., et al. (1995). Multiple defects in innate and adaptive immunologic function in NOD/LtSz-scid mice. J. Immunol. *154*, 180–191.
21. Hogan, C.J., Shpall, E.J., McNulty, O., McNiece, I., Dick, J.E., Shultz, L.D., and Keller, G. (1997). Engraftment and development of human CD34(+)-enriched cells from umbilical cord blood in NOD/LtSz-scid/scid mice. Blood *90*, 85–96.
22. Traggiai, E., Chicha, L., Mazzucchelli, L., Bronz, L., Piffaretti, J.C., Lanzavecchia, A., and Manz, M.G. (2004). Development of a human adaptive immune system in cord blood cell-transplanted mice. Science *304*, 104–107.
23. Ito, M., Hiramatsu, H., Kobayashi, K., Suzue, K., Kawahata, M., Hioki, K., Ueyama, Y., Koyanagi, Y., Sugamura, K., Tsuji, K., et al. (2002). NOD/SCID/gamma(c)(null) mouse: An excellent recipient mouse model for engraftment of human cells. Blood *100*, 3175–3182.
24. Ishikawa, F., Yasukawa, M., Lyons, B., Yoshida, S., Miyamoto, T., Yoshimoto, G., Watanabe, T., Akashi, K., Shultz, L.D., and Harada, M. (2005). Development of functional human blood and immune systems in NOD/SCID/IL2 receptor gamma chain(null) mice. Blood *106*, 1565–1573.
25. Shultz, L.D., Lyons, B.L., Burzenski, L.M., Gott, B., Chen, X., Chaleff, S., Kotb, M., Gillies, S.D., King, M., Mangada, J., et al. (2005). Human lymphoid and myeloid cell development in NOD/LtSz-scid IL2R gamma null mice engrafted with mobilized human hemopoietic stem cells. J. Immunol. *174*, 6477–6489.
26. Wege, A.K., Ernst, W., Eckl, J., Frankenberger, B., Vollmann-Zwerenz, A., Männel, D.N., Ortmann, O., Kroemer, A., and Brockhoff, G. (2011). Humanized tumor mice—a new model to study and manipulate the immune response in advanced cancer therapy. Int. J. Cancer *129*, 2194–2206.
27. Hess, M., Stritzker, J., Härtl, B., Sturm, J.B., Gentschev, I., and Szalay, A.A. (2011). Bacterial glucuronidase as general marker for oncolytic virotherapy or other biological therapies. J. Transl. Med. *9*, 172.
28. Frentzen, A., Geissinger, U., Tsoneva, D., and Stritzker, J. (2015). Use of GLV-1h68 for Vaccinia Virotherapy and Monitoring. Methods Mol. Biol. *1317*, 225–237.
29. Tsoneva, D., Stritzker, J., Bedenk, K., Zhang, Q., Frentzen, A., Cappello, J., Fischer, U., and Szalay, A.A. (2015). Drug-Encoded Biomarkers for Monitoring Biological Therapies. PLoS ONE *10*, e0137573.
30. Advani, S.J., Buckel, L., Chen, N.G., Scanderbeg, D.J., Geissinger, U., Zhang, Q., Yu, Y.A., Aguilar, R.J., Mundt, A.J., and Szalay, A.A. (2012). Preferential replication of systemically delivered oncolytic vaccinia virus in focally irradiated glioma xenografts. Clin. Cancer Res. *18*, 2579–2590.
31. Cecil, A., Gentschev, I., Adelfinger, M., Nolte, I., Dandekar, T., and Szalay, A.A. (2014). Antigen profiling analysis of vaccinia virus injected canine tumors: Oncolytic virus efficiency predicted by boolean models. Bioengineered *5*, 319–325.
32. Kober, C., Rohn, S., Weibel, S., Geissinger, U., Chen, N.G., and Szalay, A.A. (2015). Microglia and astrocytes attenuate the replication of the oncolytic vaccinia virus LIVP 1.1.1 in murine GL261 gliomas by acting as vaccinia virus traps. J. Transl. Med. *13*, 216.
33. Kober, C., Weibel, S., Rohn, S., Kirscher, L., and Szalay, A.A. (2015). Intratumoral INF-γ triggers an antiviral state in GL261 tumor cells: A major hurdle to overcome for oncolytic vaccinia virus therapy of cancer. Mol. Ther. Oncolytics *2*, Published online June 24, 2015. http://dx.doi.org/10.1038/mto.2015.
34. Wang, E., Voiculescu, S., Le Poole, I.C., El-Gamil, M., Li, X., Sabatino, M., Robbins, P.F., Nickoloff, B.J., and Marincola, F.M. (2006). Clonal persistence and evolution during a decade of recurrent melanoma. J. Invest. Dermatol. *126*, 1372–1377.
35. Sabatino, M., Zhao, Y., Voiculescu, S., Monaco, A., Robbins, P., Karai, L., Nickoloff, B.J., Maio, M., Selleri, S., Marincola, F.M., and Wang, E. (2008). Conservation of

genetic alterations in recurrent melanoma supports the melanoma stem cell hypothesis. Cancer Res. *68*, 122–131.

36. Sivori, S., Vitale, M., Morelli, L., Sanseverino, L., Augugliaro, R., Bottino, C., Moretta, L., and Moretta, A. (1997). p46, a novel natural killer cell-specific surface molecule that mediates cell activation. J. Exp. Med. *186*, 1129–1136.
37. Pessino, A., Sivori, S., Bottino, C., Malaspina, A., Morelli, L., Moretta, L., Biassoni, R., and Moretta, A. (1998). Molecular cloning of NKp46: A novel member of the immunoglobulin superfamily involved in triggering of natural cytotoxicity. J. Exp. Med. *188*, 953–960.
38. Arnon, T.I., Markel, G., and Mandelboim, O. (2006). Tumor and viral recognition by natural killer cells receptors. Semin. Cancer Biol. *16*, 348–358.
39. Strowig, T., Chijioke, O., Carrega, P., Arrey, F., Meixlsperger, S., Rämer, P.C., Ferlazzo, G., and Münz, C. (2010). Human NK cells of mice with reconstituted human immune system components require preactivation to acquire functional competence. Blood *116*, 4158–4167.
40. Ledford, H. (2015). Cancer-fighting viruses win approval. Nature *526*, 622–623.
41. Fenner, F., Henderson, D.A., Arita, I., Jezek, Z., and Ladnyi, I.D. (1988). Smallpox and Its Eradication (World Health Organization).
42. Hanahan, D., and Weinberg, R.A. (2000). The hallmarks of cancer. Cell *100*, 57–70.
43. Bergers, G., and Benjamin, L.E. (2003). Tumorigenesis and the angiogenic switch. Nat. Rev. Cancer *3*, 401–410.
44. Angarita, F.A., Acuna, S.A., Ottolino-Perry, K., Zerhouni, S., and McCart, J.A. (2013). Mounting a strategic offense: Fighting tumor vasculature with oncolytic viruses. Trends Mol. Med. *19*, 378–392.
45. Smyth, M.J., Hayakawa, Y., Takeda, K., and Yagita, H. (2002). New aspects of natural-killer-cell surveillance and therapy of cancer. Nat. Rev. Cancer *2*, 850–861.
46. Lee, S.H., Miyagi, T., and Biron, C.A. (2007). Keeping NK cells in highly regulated antiviral warfare. Trends Immunol. *28*, 252–259.
47. Koch, J., Steinle, A., Watzl, C., and Mandelboim, O. (2013). Activating natural cytotoxicity receptors of natural killer cells in cancer and infection. Trends Immunol. *34*, 182–191.
48. Beilke, J.N., Kuhl, N.R., Van Kaer, L., and Gill, R.G. (2005). NK cells promote islet allograft tolerance via a perforin-dependent mechanism. Nat. Med. *11*, 1059–1065.
49. McNerney, M.E., Lee, K.M., Zhou, P., Molinero, L., Mashayekhi, M., Guzior, D., Sattar, H., Kuppireddi, S., Wang, C.R., Kumar, V., and Alegre, M.L. (2006). Role of natural killer cell subsets in cardiac allograft rejection. Am. J. Transplant. *6*, 505–513.
50. Crome, S.Q., Lang, P.A., Lang, K.S., and Ohashi, P.S. (2013). Natural killer cells regulate diverse T cell responses. Trends Immunol. *34*, 342–349.
51. Manaster, I., Mizrahi, S., Goldman-Wohl, D., Sela, H.Y., Stern-Ginossar, N., Lankry, D., Gruda, R., Hurwitz, A., Bdolah, Y., Haimov-Kochman, R., et al. (2008). Endometrial NK cells are special immature cells that await pregnancy. J. Immunol. *181*, 1869–1876.
52. Poli, A., Michel, T., Thérésine, M., Andrès, E., Hentges, F., and Zimmer, J. (2009). CD56bright natural killer (NK) cells: An important NK cell subset. Immunology *126*, 458–465.
53. Manaster, I., and Mandelboim, O. (2010). The unique properties of uterine NK cells. Am. J. Reprod. Immunol. *63*, 434–444.
54. Yokota, M., Fukui, A., Funamizu, A., Nakamura, R., Kamoi, M., Fuchinoue, K., Sasaki, Y., Fukuhara, R., and Mizunuma, H. (2013). Role of NKp46 expression in cytokine production by CD56-positive NK cells in the peripheral blood and the uterine endometrium. Am. J. Reprod. Immunol. *69*, 202–211.
55. Puzanov, I., Milhem, M.M., Andtbacka, R.H.I., Minor, D.R., Hamid, O., Li, A., et al. (2014). Primary analysis of a phase 1b multicenter trial to evaluate safety and efficacy of talimogene laherparepvec (T-VEC) and ipilimumab (ipi) in previously untreated, unresected stage IIIB-IV melanoma. J. Clin. Oncol. (*Suppl. S5*), 32.
56. Minev, B., Kohrt, H., Kilinc, M., Chen, N., Feng, A., Pessian, M., et al. (2014). Combination immunotherapy with oncolytic vaccinia virus and checkpoint inhibitor following local tumor irradiation. J. Immunother. Cancer *2*, P112, Published online November 6, 2014. http://dx.doi.org/10.1186/2051-1426-2-S3-P112.
57. Marabelle, A., Kohrt, H., Sagiv-Barfi, I., Ajami, B., Axtell, R.C., Zhou, G., Rajapaksa, R., Green, M.R., Torchia, J., Brody, J., et al. (2013). Depleting tumor-specific Tregs at a single site eradicates disseminated tumors. J. Clin. Invest. *123*, 2447–2463.
58. Zamarin, D., Holmgaard, R.B., Subudhi, S.K., Park, J.S., Mansour, M., Palese, P., Merghoub, M., Wolchok, J.D., and Allison, J.P. (2014). Localized oncolytic virotherapy overcomes systemic tumor resistance to immune checkpoint blockade immunotherapy. Sci. Transl. Med., Published online: March 5, 2014. http://dx.doi.org/10.1126/scitranslmed.3008095.
59. Brehm, M.A., Wiles, M.V., Greiner, D.L., and Shultz, L.D. (2014). Generation of improved humanized mouse models for human infectious diseases. J. Immunol. Methods *410*, 3–17.
60. Tanaka, S., Saito, Y., Kunisawa, J., Kurashima, Y., Wake, T., Suzuki, N., Shultz, L.D., Kiyono, H., and Ishikawa, F. (2012). Development of mature and functional human myeloid subsets in hematopoietic stem cell-engrafted NOD/SCID/IL2rγKO mice. J. Immunol. *188*, 6145–6155.
61. Gille, C., Orlikowsky, T.W., Spring, B., Hartwig, U.F., Wilhelm, A., Wirth, A., Goecke, B., Handgretinger, R., Poets, C.F., and André, M.C. (2012). Monocytes derived from humanized neonatal NOD/SCID/IL2Rγ(null) mice are phenotypically immature and exhibit functional impairments. Hum. Immunol. *73*, 346–354.
62. Grosso, J.F., and Jure-Kunkel, M.N. (2013). CTLA-4 blockade in tumor models: An overview of preclinical and translational research. Cancer Immun. *13*, 5.
63. Fecci, P.E., Ochiai, H., Mitchell, D.A., Grossi, P.M., Sweeney, A.E., Archer, G.E., Cummings, T., Allison, J.P., Bigner, D.D., and Sampson, J.H. (2007). Systemic CTLA-4 blockade ameliorates glioma-induced changes to the CD4+ T cell compartment without affecting regulatory T-cell function. Clin. Cancer Res. *13*, 2158–2167.
64. Vudattu, N.K., Waldron-Lynch, F., Truman, L.A., Deng, S., Preston-Hurlburt, P., Torres, R., Raycroft, M.T., Mamula, M.J., and Herold, K.C. (2014). Humanized mice as a model for aberrant responses in human T cell immunotherapy. J. Immunol. *193*, 587–596.
65. Falkner, F.G., and Moss, B. (1990). Transient dominant selection of recombinant vaccinia viruses. J. Virol. *64*, 3108–3111.
66. Waine, G.J., Becker, M.M., Scott, J.C., Kalinna, B.H., Yang, W., and McManus, D.P. (1994). Purification of a recombinant Schistosoma japonicum antigen homologous to the 22-kDa membrane-associated antigen of S. mansoni, a putative vaccine candidate against schistosomiasis. Gene *142*, 259–263.
67. Hanson, D.C., Neveu, M.J., Mueller, E.E., Hanke, J.H., Gilman, S.C., Davis, C.G., et al. (2004). Human monoclonal antibodies to CTLA-4. Abgenix, Inc., Fremont, California; Pfizer Inc., Fremont, California United States Patent. U.S. patent 6,682,736; U.S. patent 7,807,797; U.S. patent 7,824,679; and U.S. patent 8,143,379.
68. Joklik, W.K. (1962). The purification fo four strains of poxvirus. Virology *18*, 9–18.
69. Dias, J.D., Hemminki, O., Diaconu, I., Hirvinen, M., Bonetti, A., Guse, K., Escutenaire, S., Kanerva, A., Pesonen, S., Löskog, A., et al. (2012). Targeted cancer immunotherapy with oncolytic adenovirus coding for a fully human monoclonal antibody specific for CTLA-4. Gene Ther. *19*, 988–998.